# Seismic images of crustal duplexing and continental subduction in the Brooks Range

E.S. Wissinger and A. Levander
Department of Geology and Geophysics, Rice University, 6100 Main St., Houston, Texas

Nikolas I. Christensen
Department of Earth and Atmospheric Sciences, Purdue University, West Lafayette, Indiana

**Abstract.** We have interpreted an integrated vertical incidence to wide-angle seismic data set to develop a consistent migrated seismic reflection image and seismic velocity model of the Brooks Range fold and thrust belt in north central Alaska. The common midpoint (CMP) reflection data image the principal structures comprising the Brooks Range: the Endicott Mountains allochthon (EMA), the crustal scale Doonerak duplex, the master detachment, a 1.0-1.5 s thick zone of lower crustal reflectivity just above the crust-mantle boundary, and a complex crustal root. The master detachment separates the crust into units which have been uplifted and deformed in the fold and thrust belt from those which have not. Least squares inversion of both reflection and refraction travel time data produced a velocity model consistent with the CMP image of the Brooks Range as well as with the Bouguer gravity data. The different layers comprising the seismic velocity model correlate well with the principal structural elements identified in the seismic reflection data, and seismic velocities in the model compare favorably to petrophysical data from Brooks Range rock samples. Maximum crustal thickness in the Brooks Range is 49 km, at an asymmetric root located under the EMA. At the root we observe an offset in the lower crustal reflectivity and two deep zones of reflections north of the root. We interpret these as a Moho offset of some 5 km near the range front, which in our favored interpretation resulted from subduction of the Brooks Range lower crust northward beneath the North Slope. A mantle reflective zone which we interpret as the subducted lower crust can be traced to depths as great as 65 km. Above this zone at considerably shallower depth is the original North Slope Moho. Proximity of the continental subduction zone to the crustal scale Doonerak duplex suggests that the development of the fold and thrust belt has been at least partially controlled by the lower crust/mantle subduction.



## Introduction

In the last decade the Trans-Alaska Lithospheric Investigation Program (TALI) has acquired detailed geological and seismic data along a 1400 km long corridor crossing Alaska called the Trans-Alaska Crustal Transect (TACT [See *Stone et al.*, 1986]). The TACT corridor extends along the Trans-Alaska pipeline from the Gulf of Alaska through the various allochthonous terranes comprising southern, central, and northern Alaska, including the Brooks Range and associated terranes in northern Alaska. The transect ends on the North Slope over what is believed to be the proto-North American craton (Figure 1). TACT is unique in that it extends from an active convergent margin where the Pacific plate is subducting beneath southern Alaska to a rifted passive margin forming the northern edge of the North American craton at the Arctic Ocean.

In this paper we describe the interpretation of the vertical incidence to wide-aperture seismic profile crossing the Brooks Range fold and thrust belt, as well as the Ruby terrane and the Yukon-Koyukuk basin to the south and the Colville basin and North Slope to the north (Figure 1). Preliminary interpretations of the seismic reflection and wide-aperture data including balanced and partially balanced cross sections have been reported previously [*Levander et al.*, 1994; *Fuis et al.*, 1995; *Wissinger*, 1995]. A series of detailed balanced cross sections have been derived from the reflection data [*Wissinger*, 1995; *Wissinger et al.*, 1997]. Here we review the principal seismic findings already published and present a new seismic velocity model and gravity models for the Brooks Range. The seismic velocity model is compared to laboratory measured velocities made on Brooks Range rocks. We also present and interpret new common midpoint (CMP) reflection data showing upper mantle vertical-incidence reflections beneath the northern Brooks Range and Colville basin.

## Geologic Overview and Previous Seismic Results

The Brooks Range, one of the northernmost elements of the North American Cordillera, is a Jurassic-Recent aged, east-west trending, north vergent fold and thrust belt located in north central Alaska (Figure 1). An excellent review of the development of the fold and thrust belt is given by *Blythe et al.*, [1996] which we summarize here. In the Jurassic, the southern edge of the Alaskan North American craton was a passive continental margin. In the Late Jurassic (prior to 160 Ma) through Early Cretaceous this passive margin was shortened by collision with an island arc, forming the Brooks Range and its corresponding foredeep, the Colville basin. Remnants of this island arc, which were accreted to the southern Alaska margin by 130-100 Ma, are now found in the Yukon-Koyukuk basin on the southern flank of the Brooks Range. The southern part of the range experienced variable and debated amounts of extension in the period 130-90 Ma [*Gottschalk and Oldow*, 1988; *Miller and Hudson*, 1991; *Till et al.*, 1993]. In our study area, along the TACT transect, extension appears to be relatively minor. Significant elements of the Brooks Range were again shortened in the Tertiary between 60 Ma and 25 Ma, possibly resulting from low-angle subduction of the Kula plate along the north dipping southern Alaska subduction zone.

The Brooks Range is largely composed of deformed passive margin sediments of mid-Paleozoic age that have been overthrust by ophiolitic rocks of the Angayucham terrane, during the collision of the Koyukuk arc [*Mull,* 1982]. Metamorphic grade increases from north to south from relatively undeformed rocks in the Colville basin and foreland to greenschist and higher facies in the schist belt located in the southern part of the range. The assemblages of the Brooks Range and North Slope are subdivided into a number of major thrust-bounded terranes and subterranes based on similarities in structure, stratigraphy, and/or metamorphism (Figure 1). Different nomenclatures are in use to describe these terranes, one by a number of researchers including *Jones et al.* [1987] and *Moore et al.* [1994] and one by *Oldow et al.* [1987]. The latter is more in keeping with traditional concepts developed for fold and thrust belts, whereas the former is more in keeping with the terrane accretion concepts developed for western North America, with the result that some differences exist in the intent of the definitions. We summarize the nomenclatures in Table 1. Here we describe the rock units crossed by our seismic line from north to south. (1) The Colville basin is the Jurassic-Recent foreland succession composed of foredeep sediments shed from the rising Brooks Range. (2) The Endicott Mountains allochthon (EMA) is a Devonian-Mississippian succession of clastics, volcaniclastics, conglomerates and carbonates. (3) The Doonerak window exposes the Doonerak duplex and related thrust structures, consisting of lower Paleozoic to Triassic south dipping imbricates composed of phyllite, argillite, and volcanic rocks of the Devonian-Jurassic passive margin. (4) The Skajit allochthon [*Oldow et al.*, 1987] or Hammond subterrane [*Moore and Mull*, 1989] is a structurally complex assemblage of metamorphosed Cambrian-Devonian clastics and carbonates. (5) The schist belt [*Oldow et al.*, 1987] or Coldfoot subterrane [*Moore et al.*, 1992] is a highly deformed quartz-mica schist which has undergone greenschist, amphibolite, and blueschist facies metamorphism [*Gottschalk*, 1987]. (6) The Rosie Creek allochthon [*Oldow et al.*, 1987] or Slate Creek subterrane [*Moore et al.*, 1992] is a low grade metamorphic assemblage composed of Cambrian-Silurian clastic and carbonate rocks. (7) The southernmost terrane of the Brooks Range proper in our study area is the Angayucham terrane, obducted Devonian to mid-Jurassic ophiolitic rocks. South of the Brooks Range are (8) the Yukon-Koyukuk basin, a triangular lowland containing a structural high of volcanic rocks flanked by 5-8 km of mid-Cretaceous-Recent terrigenous sediments [*Box and Patton*, 1985], and (9) the Ruby terrane, a linear uplift trending diagonally across central Alaska composed of Paleozoic continental and island arc rocks and Cretaceous plutons.

The seismic reflection data from the Brooks Range survey have provided a link between surface mapping and the structure of the upper and middle crust, through identification of major crustal units and detachment faults which permitted reconstructions of the development of the fold and thrust belt (Figure 2) [*Levander et al.*, 1994; *Fuis et al.*, 1995; *Wissinger*, 1995; *Blythe et al.*, 1996; *Wissinger et al.*, 1997]. We reference the seismic reflection data and the velocity model (described in the next two sections) to model coordinates, denoted by KM, with 0 KM at the Arctic Circle. The preservation of stratigraphy and the manner and degree of deformation strongly affect seismic reflection character. Where stratigraphy is well preserved and rocks deformed by brittle failure and folding, such as in the EMA and the Doonerak duplex (180-295 KM), the seismic reflection section contains long bright, continuous reflections. In contrast, where no recognizable stratigraphy exists and the rocks appear to be ductilely deformed, as in the schist belt [*Gottschalk,* 1990], seismic reflections are short, weak, and chaotic (160-180 KM). This is likely a result of multiscaled fabrics and seismic velocity and lithologic heterogeneity [see *Levander et al.*, 1994].

In the seismic reflection data, we have interpreted the bottom of a continuous series of reflections in the crust as the basal decollement at upper/midcrustal depths in the northernmost range (~12 km) which deepens to lowercrustal depths (~28 km) beneath the schist belt (170-295 KM, Figure 2; see also Figure 2 of *Levander et al.* [1994]. Our interpretation of the seismic reflection packages above the decollement suggests that the northern Brooks Range has formed from the emplacement of relatively thin thrust sheets above this detachment [*Wissinger*, 1995]. These thrust sheets are generally thinner in the northern than in the southern part of the range, nowhere exceeding 10 km, and have aspect ratios greater than 3 (horizontal/vertical).

**Table 1.** Nomenclatures Used

| Lithotectonic Assemblages | Terranes and Subterranes | Geologic Provinces |
|---|---|---|
| 1, Colville basin | Colville basin | foreland belt |
| 2, Endicott Mnts. allochthon | Endicott Mnts. subterrane | crestal belt |
| 3, Doonerak window | North Slope subterrane | central belt |
| 4, Skajit allochthon | Hammond subterrane | central belt |
| 5, schist belt | Coldfoot subterrane | schist belt |
| 6, Rosie Creek allochthon/phyllite belt | Slate Creek and Prospect Creek subterranes | phyllite belt |
| 7, Angayucham terrane | Angayucham terrane | greenstone belt |
| 8, Yukon-Koyukuk depression | Yukon-Koyukuk basin | Yukon-Koyukuk basin |
| 9, Ruby terrane | Ruby terrane | Ruby terrane |

Lithotectonic assemblages from *Oldow et al.* [1987]; terranes and subterranes from *Jones et al.* [1987] and *Moore et al.* [1994]; and geologic provinces from *Till et al.* [1988] and *Moore et al.* [1994].

An important seismic observation is the 1.0 to 1.5 s thick complex zone of reflections in the lower crust beneath most of the Brooks Range (from 130 to 265 KM), the base of which we interpret to be the Moho (Figure 2), this has been confirmed by analysis of the wide-angle seismic data described below. We also observe an apparent offset in these reflections from the Moho of 2.0 s (~6-10 km) beneath the EMA near the northern range front (275 KM). To the north (275-295 KM), the lower crustal reflections are ~3.0 s thick. Here also we interpret the base of the reflectivity as the Moho. The reflection section shows an asymmetric crustal root near the northern range front beneath the EMA.

Estimates of shortening across the entire range from balanced cross sections using the 1990 reflection data are 500 to 600 km, if one includes the metamorphic belts in the southern Brooks Range in the reconstructions (Plate 1) [see *Wissinger*, 1995; *Wissinger et al.*, 1997]. Shortening based on the preserved stratigraphy in the EMA and North Slope is 125-150 km [*Oldow et al.*, 1987; *Wissinger*, 1995; *Wissinger et al.*, 1997; *Blythe et al.*, 1996].

## Seismic Data

The 1990 seismic experiment was designed to obtain both a reflection image and a crustal velocity profile from the surface to the base of the crust [*Murphy et al.*, 1993; *Levander et al.*, 1994; *Fuis et al.*, 1995]. Details of the processing of the seismic reflection data are given elsewhere [*Levander* et al., 1994; *Wissinger*, 1995]. Here we schematically describe the seismic reflection data processing and the interplay between the reflection processing and the travel time velocity inversion. We first produced a brute stack near-vertical reflection image, and a seismic velocity model from inversion of *Pg* travel times. We next used the preliminary velocity model to restack the seismic data to form a clearer image of the principal structures of the range, and to construct line drawing depth migrations (Plate 1) [*Raynaud*, 1988; *Holliger and Kissling*, 1991]. The most prominent reflections we interpret as likely seismic velocity boundaries, which we use as a priori information for assigning boundaries in the travel time inversion for the entire crust (Figure 4a). The final velocity model was then used to remigrate the seismic reflection data. The data set has been used in a consistent manner to develop a unified reflection image and seismic velocity model. We note that the reflection and refraction images provide complementary pictures of the crust: The reflection image is a high-frequency backscatter image of impedance contrasts in the crust, whereas the velocity model is a smoother image derived from transmitted and reflected energy.

We have used travel times from *Pg*, *PmP*, and *Pn* phases and reflection travel times from numerous intracrustal near-vertical and wide-angle reflections from 42 shot records to develop the velocity model. The field data were densely recorded in five overlapping and abutting deployments of 700 vertical component seismic channels, with channels nominally spaced at 100 m. A number of shot points were fired into more than one deployment, forming continuous shot records with offsets as great as 212 km (Figure 3a-3d). Most of the long offset shot records show strong *PmP* reflections that can be traced with confidence from near vertical incidence to large offsets, thus spanning the precritical and postcritical ranges (Figure 3a-3d). Two of the shots produced clear *Pn* arrivals at offsets greater than 150 km. Many more travel times are available for each phase than were used in the inversions. We identified no intracrustal refraction events other than *Pg*.

Determining the across strike crustal velocity structure of the fold and thrust belt using ray tracing can be difficult due to rapid vertical and lateral spatial velocity variation. The a priori data provided by the migrated CMP section provided interface control points to stabilize the inversion across the structurally complex folded belt. We used the two-dimensional ray-based method of *Zelt and Smith* [1992] to invert the travel time picks. Inversion of the data was performed layer by layer from top to bottom, simultaneously

incorporating both reflection and refraction travel times. During each inversion iteration, both the values of velocity and depth nodes were allowed to vary. We emphasize that we included reflection travel times from all major intracrustal boundaries in the seismic velocity inversion (Figures 4a and 4b, Plate 2). The underlying assumption in the velocity model we have developed is that the principal structural elements of the range identified by prominent reflections are also layer boundaries of the seismic velocity model.

## Velocity Model and Interpretation

The eight-layer velocity model derived from the travel time inversion is shown in Figures 4a and 4b. A plot of the velocity and depth node parameterization is given in Figure 4b. The model was parameterized with two velocity and depth nodes per shot point interval in the shallowest layers, with the number of nodes decreasing with depth. Velocity model resolution is described in the appendix. The seismic boundaries identified utilizing the seismic reflection data are the tops of layers 2, 3, 4, 5, 6, 7, and 8 as shown in Figures 4a and 5.

The ray diagrams and travel time fits used in the inversion for seismic velocities and boundary depths are shown in Figures 5a-5i. Velocity depth profiles at a number of locations in the velocity model are compared to laboratory measurements of seismic velocity made on Brooks Range rock samples in Figure 6. The rock physics data used in this paper are summarized in Table 2. Several of the layers represent more than one terrane and have large lateral variations in velocity. Some layers are continuous across terrane boundaries as a consequence of the model parameterization in which a minimal number of layers are used to represent the velocity structure. This is an inherent problem with using ray-based methods to model wave propagation in complex structures. All lithotectonic assemblages exposed at the surface have other assemblages beneath them, expected from the stacking of thrust sheets during formation of the fold and thrust belt. Velocity depth functions are interpreted in terms of petrophysical measurements made in lithologies from the different terranes.

In the crust above layer 6, approximately 4300 *Pg* travel times from 42 shot gathers were inverted for seismic velocity to depths of at most 15 km. Turning rays penetrated layers 1, 2, 3, and 5 (Figures 5a and 5b), but not layer 4 at the south end of the study area, nor layer 6. Following inversion for first arrivals, reflection times were inverted with refraction times to fix the velocity model boundaries corresponding to the tops of layers 2-6 (Figures 5c-5f). *Pg* phases were weighted more heavily (±50 ms) than shallow to intermediate crustal reflections (±150 ms) in the inversions. Travel time fits for the *Pg* arrivals are shown in Figures 5a and 5b. Dense *Pg* ray coverage provided good velocity constraint from the surface to approximately 10 km depth throughout the range (layers 1-3 and 5) with velocities in the center of the Brooks Range known to ±0.05 to ±0.10 km/s (Figures 5a and 5b). Travel time residuals for inversions for each layers are given in Table 3. The structure of the middle and lower crust and upper mantle is known from inversion of 600 travel times of precritical and postcritical *PmP* phases from six shots and 30 *Pn* travel times from two large offset shots. Velocities are known to ±0.20 km/s. The travel time residual for the lower crust is 0.19 s, while that for the upper mantle *Pn* phases is 0.20 s.

In addition to the turning rays and reflections, in several layers we also observe numerous internal reflections too complicated to model as many individual layers. Reflections internal to a layer were inverted as "floating reflectors." Floating reflectors are ray theoretically positioned within the layer following the inversion for velocity [*Zelt and Forsythe*, 1994] and provide a means of modeling reflections which result from local impedance contrasts rather than bulk velocity contrasts without increasing the number of velocity layers in the model. In layer 5 we have modeled 10 floating reflectors as "ramp and flat" structures (Figures 4a and 5g). Similarly, we have modeled the top of the reflective zone above the Moho and one reflection from beneath the Moho, as floating reflectors, as shown in Figures 4a and 5i.

## Interpretation

As in previous interpretations of the seismic reflection data [*Levander et al.*, 1994; *Fuis et al.*, 1995; *Wissinger*, 1995], we interpret a number of the prominent reflections in the CMP section as directly associated with boundaries of lithotectonic assemblages. These reflection events correspond to the reflection travel times we have used to position layer boundaries in the seismic velocity model (Figure 4a). Specifically, we interpret (1) the base of layer 2 from 238 to 310 KM as the base of the EMA, (2) the top of layer 5 as the top of the Doonerak duplex, and (3) the top of layer 6 as the location of a basal decollement (Figure 4a). The detachment is poorly imaged beneath the schist belt, likely resulting from the small velocity contrast between the rocks of layers 5 and 6 in the southern part of the range. Further, from both the near-vertical and the wide-angle *PmP* reflection data, we interpret the bottom of layer 6 as the Moho (Figures 2 and 3a-3d). A 1.0-1.5 s zone of high reflectivity is apparent in the lowermost crust south of the crustal root at 265 KM, whereas north of 265 KM the lower crustal reflectivity is 3.0 s thick. We discuss the velocity structure layer by layer from the shallow crust to the upper mantle.

## Colville Basin

Layer 1, the shallowest layer, corresponds to the sediments of the Colville basin, the alluvial and glacial deposits

Table 2. Laboratory Velocities

| Samples | Density, g/cm3 | *P* Velocity at Pressure, MPa 10 | 50 | 100 | 200 | 400 | 600 | 800 | 1000 |
|---|---|---|---|---|---|---|---|---|---|
| A-71 average - schist (schist belt) 66.355°N, 150.080°W | 2.765 | 5.507 | 6.001 | 6.226 | 6.375 | 6.475 | 6.531 | 6.571 | 6.602 |
| TA-71 A axis | 2.750 | 4.168 | 4.979 | 5.344 | 5.573 | 5.720 | 5.802 | 5.861 | 5.907 |
| TA-71 B axis | 2.746 | 6.036 | 6.382 | 6.544 | 6.657 | 6.735 | 6.778 | 6.808 | 6.831 |
| TA-71 C axis | 2.799 | 6.319 | 6.642 | 6.790 | 6.895 | 6.971 | 7.014 | 7.044 | 7.068 |
| TA-72 average - marble (Skajit) 67.856°N, 148.822°W | 2.691 | 6.047 | 6.314 | 6.463 | 6.575 | 6.632 | 6.656 | 6.672 | 6.685 |
| TA-73 average - phyllite (EMA) 67.95°N, 149.77°W | 2.739 | 5.514 | 5.835 | 5.991 | 6.125 | 6.223 | 6.293 | 6.335 | 6.369 |
| TA-74 average - conglomerate (EMA) 68.13°N, 149.49°W | 2.664 | 5.610 | 5.793 | 5.874 | 5.957 | 6.042 | 6.091 | 6.127 | 6.154 |
| TA-75 average - phyllite (EMA) 68.15°N, 149.44°W | 2.736 | 5.659 | 5.785 | 5.840 | 5.905 | 5.981 | 6.027 | 6.060 | 6.085 |
| TA-76 average - conglomerate (EMA) 68.32°N, 129.35°W | 2.609 | 5.038 | 5.446 | 5.653 | 5.821 | 5.940 | 6.003 | 6.047 | 6.082 |
| TA-77 average - quartzite (North Slope) 68.13°N, 149.46°W | 2.808 | 5.616 | 5.980 | 6.136 | 6.252 | 6.347 | 6.402 | 6.441 | 6.472 |
| TA-79 average - marble (Skajit) 67.58°N, 149.58°W | 2.654 | 5.484 | 6.063 | 6.370 | 6.592 | 6.712 | 6.764 | 6.800 | 6.828 |
| TA-80 average - schist (schist belt) 67.28°N, 150.26°W | 2.657 | 4.901 | 5.393 | 5.666 | 5.910 | 6.086 | 6.171 | 6.230 | 6.277 |
| TA-80 A axis | 2.659 | 4.057 | 4.711 | 5.077 | 5.418 | 5.672 | 5.800 | 5.889 | 5.958 |
| TA-80 B axis | 2.654 | 5.411 | 5.796 | 6.007 | 6.187 | 6.306 | 6.362 | 6.401 | 6.431 |
| TA-80 C axis | 2.652 | 5.409 | 6.163 | 6.512 | 6.702 | 6.783 | 6.822 | 6.850 | 6.871 |
| TA-82 average - limestone (EMA) 67.92°N, 150.58°W | 2.656 | 5.395 | 5.786 | 5.980 | 6.141 | 6.258 | 6.319 | 6.361 | 6.394 |
| TA-83 average - phyllite (Doonerak) 67.90°N, 150.59°W | 2.684 | 5.623 | 5.789 | 5.865 | 5.950 | 6.050 | 6.115 | 6.163 | 6.200 |
| TA-84 average - greenstone (Doonerak) 67.906°N, 150.594°W | 2.943 | 6.417 | 6.577 | 6.653 | 6.736 | 6.820 | 6.867 | 6.899 | 6.992 |
| TA-88 average - limestone (North Slope) 68.44°N, 149.34°W | 2.621 | 5.076 | 5.669 | 5.987 | 6.223 | 6.355 | 6.417 | 6.460 | 6.494 |
| TA-89 average - argillite (North Slope) 68.45°N, 149.32°W | 3.069 | 5.845 | 6.024 | 6.125 | 6.239 | 6.346 | 6.397 | 6.427 | 6.448 |
| TA-90 average - siltstone (North Slope) 68.46°N, 149.36°W | 2.642 | 4.881 | 5.162 | 5.303 | 5.460 | 5.662 | 5.712 | 5.772 | 5.816 |
| TA-91 average - siltstone (North Slope) 68.72°N, 149.02°W | 2.661 | 4.582 | 5.061 | 5.298 | 5.503 | 5.671 | 5.764 | 5.830 | 5.883 |
| TA-93 average - quartz-mica schist (Doonerak) 67.41°N, 150.27°W | 2.708 | 5.198 | 5.845 | 6.054 | 6.147 | 6.207 | 6.241 | 6.266 | 6.285 |

Velocities in kilometers per second

**Table 3.** Travel Time Residuals

| Phase | Layer | Number of Observations | RMS Misfit ms | Normalized $x^2$ | Model Parameters Constrained Velocity/ Boundary Nodes |
|---|---|---|---|---|---|
| *Pg* | 1-5 | 6496 | 98 | 3.25 | 135* / 66 |
| *Pn* | 7 | 58 | 124 | 1.70 | 6 / - |
| *PmP* | base layer 6 | 609 | 177 | 1.81 | 16 / 14 |
| Reflection | floating; upper crust | 2233 | 147 | 0.84 | — / 43 |
| Reflection | floating; lower crust | 553 | 108 | 0.33 | — / 12 |
| Reflection | base layer 1 | 269 | 78 | 0.61 | 28* / 12 |
| Reflection | base layer 2 | 1397 | 89 | 0.79 | 54* / 25 |
| Reflection | base layer 3 | 1650 | 123 | 1.46 | 40* / 28 |
| Reflection | base layer 5 | 621 | 145 | 1.87 | 10*/ 14 |
| Total | | 13886 | | | 289 / 214 |

* Pg was inverted simultaneously with reflections from the base of layers 1-5.



and the uppermost crust within the Brooks Range, and the sediments of the Yukon-Koyukuk basin (Figures 4, 5a, 5b, and 6 ). In the two basins the base of layer 1 was constrained by reflections from seven shots (Figure 5b).

The Brookian and Ellesmerian (all post-Late Devonian) sedimentary rocks above the acoustic basement are represented by layers 1 and 3 from 320 to 400 KM: mean velocity is 4.48 ±0.05 km/s, ranging from 3.76 km/s at the surface to 5.40 km/s at the base of the layer 1, and as high as 5.57 km/s at the base of layer 3 (Figures 4 and 6). These velocities are intermediate between sonic velocities measured in North Slope wells which show nearly linear velocity gradients (Figure 6a) [*Hawk*, 1985] and the somewhat higher velocities predicted from laboratory data (Figure 7a).

## Endicott Mountains Allochthon

In the Brooks Range proper (EMA, Doonerak region and metamorphic terranes) layer 1 is substantially thinner (1.0-1.5 km thick) than in the flanking basins, with an average velocity of 4.85 ±0.05 km/s. Velocities in this layer agree well with the refraction velocities observed in short-offset (625-725 m) noise spreads shot during the 1988 pilot experiment. We attribute these velocities to refractions in the permafrost layer and the shallowmost crust [*Lafond et al.*, 1988].

The EMA is represented by layer 2 north of the Doonerak region (300 KM to 240 KM). Despite being a complexly deformed thrust package, the EMA is well defined in both the reflection image and the travel time inversion. We interpret the bottom of the layer as the base of a subhorizontal zone of reflectivity that extends from 260 KM to 300 KM (Figures 2 and 4). Velocities of 5.60 to 5.80 ±0.05 km/s are measured in the EMA and compare extremely well to laboratory measurements of EMA rocks (Figure 6b). Beneath the EMA, layer 3 occupies the region between the EMA and the basal decollement. Reflection travel times from 12 shot records were used to define the base of this layer (Figures 4a and 5e). Seismic velocity in layer 3 is both laterally and vertically variable and ranges from 5.83 to 6.30 km/s (Figures 4 and 6). The ray diagrams show that the sub-EMA layer is well sampled by turning rays from four shots. Rocks in this region have been hypothesized to be Cretaceous foredeep sediments incorporated along the range front during orogenesis [*Oldow et al.*, 1987, *Wissinger*, 1995], basement-cored anticlinoria associated with Cenozoic compression [*Wallace and Hanks*, 1990, *Fuis et al.*, 1995, *Wissinger*, 1995], or deeper imbricates of EMA rocks [*Blythe et al.*, 1996]. The rock physics data suggest that autochthonous North Slope sedimentary rock velocities are somewhat too low, EMA velocities are slightly too low, and Doonerak lithology velocities are somewhat too high compared to the observed velocities. Therefore layer 3 could consist of (1) only high-velocity Brookian sedimentary rocks, (2) Brookian (post-Jurassic) sedimentary rocks which have been substantially metamorphosed, (3) a mix of post-Devonian sedimentary rocks and basement rocks, both involved in shortening, or (4) additional EMA rocks. Hypotheses 1 and 2 seem unlikely: The first would be coincidental unless unusually large amounts of carbonates comprise most of layer 3. The second is unlikely as rocks at similar depth in the Colville basin have substantially lower velocities in our seismic velocity model (a maximum of 5.57 ±0.20 km/s from 320 KM to 400 KM). Basement velocities beneath the Colville basin and subdecollement velocities are substantially higher (6.40-6.50 km/s) than in the sub-EMA rocks (5.99-6.12 km/s), suggesting that layer 3 is unlikely to be composed solely of base-

**Table 4.** Density Values

| Terrane | Seismic Model Layer | Measured Density, $10^3$ kg/m$^3$ | Model 1 | Model 2 | Model 3 |
|---|---|---|---|---|---|
| EMA | 2 and 3 | 2.61-2.74 | 2.51-2.70 | 2.54-2.75 | 2.53-2.71 |
| Doonerak | 5 | 2.68-2.94 | 2.76 | 2.75 | 2.75 |
| Skajit* | 2 | 2.65-2.69 | 2.65 | 2.66 | 2.66 |
| Schist | 2 and 3 | 2.66-2.77 | 2.76-2.78 | 2.75-2.76 | 2.75-2.76 |
| Middle Crust | 6 | N/A | 2.76 | 2.75 | 2.75 |
| Lower crust | - | N/A | N/A | 2.90 | 2.90-3.20 |
| Upper mantle | 7 and 8 | N/A | 3.25-3.35 | 3.31-3.40 | 3.31-3.40 |



ment rocks. If the rocks of layer 3 are EMA lithologies (hypothesis 4), then they were overridden by a coherent thrust sheet of additional EMA rocks whose base gives rise to the reflection events at 5.0-6.0 km depth. We think that balanced cross sections in which the EMA is thrust atop relatively undeformed Brookian sedimentary rocks are incorrect as are cross sections in which the EMA overrode deformed basement rocks. They most likely appear to be cross sections in which combinations of post-Jurassic sedimentary rocks, basement rocks, and other EMA units are included [e.g., *Blythe et al.*, 1996; *Wissinger et al.*, 1997].

## Doonerak Duplex

The Doonerak window is a basement exposure some 20 km west of the seismic line. Along the seismic profile the top of the Doonerak duplex, corresponding to the along strike projection of the Doonerak window, is overlain by EMA rocks to depths of 4.8 km (Figure 6c). In the velocity model, layer 2 represents the EMA, and layer 5 is composed only of rocks internal to the Doonerak duplex (110 KM to 263 KM). Velocities in layer 5 range from 6.37 to 6.56 ±0.20 km/s and are only slightly lower than velocities observed deeper in the crust (Figures 4 and 6). The base of layer 5 was constrained by reflections from eight shots. We interpret the bottom of layer 5 as the basal decollement surface. This layer deepens from 19 km depth at 260 KM to 28 km depth at 110 KM (Figure 5f). Laboratory velocities in phyllite and greenstone from the Doonerak window show velocities from 6.05 to 6.20 and 6.74 to 6.92 km/s in the appropriate depth ranges. The average of these velocities agrees well with the seismic observations (Figure 6c).

Three shots illuminated a single 10 km long south dipping floating reflector which we have interpreted as being the subsurface expression of a thrust fault mapped in the Doonerak window (Plates 1 and 2, and Figure 5g).

## Skajit Allochthon and Schist Belt

In the central and southern Brooks Range, layer 2 is composed of rocks of the Skajit allochthon (240 KM to 185 KM) and the schist belt (185 KM to 160 KM). The base of the Skajit (layer 2, Figure 6d) is defined at 3-4 km depth on the basis of shallow reflection data [*Wissinger et al.*, 1997]. We have interpreted the Skajit as a relatively thin unit with seismic velocity 6.10 ±0.10 km/s, overlying schist belt rocks in layer 3 (Figures 4 and 6).

In the schist belt (near 125 KM) the base of the layer 2 is defined by a variably dipping zone of discontinuous reflections (Figure 2). We interpret layer 3 south of the Doonerak region as also being schist belt rocks, which lie beneath the surface exposures of the Skajit and schist belt. Reflections from 11 shots define the base of layer 3 south of the Doonerak, corresponding to the top of the Doonerak duplex (230 KM to 135 KM) and to an unknown unit in the southern part of the range (from 135 KM to the south). The schist belt rocks in layers 2 and 3 increase in velocity from 5.60 to 6.17 and 6.42 to 6.45 (Figures 6e and 6f).

Seismic velocities measured in situ are comparable to laboratory measurements of Skajit rocks and schist belt rocks in layer 2 (Table 2) . However, neither schist belt nor Skajit rock velocities agree with the in situ velocities measured in layer 3; the former are too low, and the latter is too high (Figures 6d-6f). This is possibly explained as resulting from anisotropy in layer 3, as schist belt rocks exhibit anisotropy of 13 to 21% in the depth range of layer 3 (Figure 6f and

Table 2). Another possibility is that this region is more structurally complex than we have modeled it.

## Southern Terranes

In the Rosie Creek allochthon, Angayucham terrane, and Yukon-Koyukuk basin the mean surface layer velocity is 5.10 ±0.05 km/s with velocities as low as 4.09 km/s at the surface to 5.70 km/s at 2.80 km depth (Figure 4).

Seismic velocity in layer 2 in the Ruby terrane (100 KM to the south) is 5.60 ±0.10 km/s. Beneath layer 2 in the southern part of the range, layer 4 is a geologically unknown unit. The northern boundary of layer 4 is well delineated by a ~15 km long north dipping reflector imaged beneath the Yukon-Koyukuk basin (140 KM to 125 KM, Figure 2). Otherwise neither the geometry nor the velocity of layer 6 are well constrained by the seismic data. We interpret the base of the layer 4 as the continuation of the basal decollement to the south

The origin and significance of the north dipping reflector at 125 KM to 140 KM at depths of 15-20 km are unclear (Figure 2). *Fuis et al.* [1995] have proposed that the reflector represents the leading edge of another crustal duplex which formed during Mesozoic compression. Alternatively it could be associated with a north dipping backthrust zone internal to the schist belt and southern Doonerak duplex.

## Middle and Lower Crust

Layer 6 represents the middle and lower crust beneath the Colville basin and the EMA and the lower crust beneath the crystalline terranes of the southern Brooks Range. Velocities range from 6.22 to 6.58 ±0.20 km/s. The crust beneath the detachment shows a slow increase in average velocity southward from the North Slope to the Brooks Range (from 6.39 to 6.55 km/s; Figure 4). The base of this layer forms an asymmetric crustal root, with a maximum depth of 49 km beneath the EMA at 265 KM. From the south the Moho deepens with increasing dip from 35 km beneath the Ruby terrane to 49 km beneath the EMA. From the north the Moho deepens from 36 km beneath the North Slope to 49 km beneath the EMA.

The CMP data show a 1.0 to 2.0 s zone of reflectivity above the Moho south of the root zone (Figures 2 and 4). A similar but thicker (~3.0 s) reflective zone is observed north of the crustal root (290 KM to 340 KM) and is offset from the southern zone by 1.5 to 2.0 s (~5.0-6.5 km). We have modeled the top of the reflective zones as two floating reflectors, one to the south of the crustal root and one to the north (Plate1). We interpret the base of each reflective zone as the Moho and the top of it (the position of the floating reflectors) as the top of the lowermost crust. The southern floating reflector is 4.0 to 5.0 km above the Moho, the northern floating reflector is 8.0 to 9.0 km above the Moho.

## Mantle Velocities and Reflections

Upper mantle velocity in layer 7 is known beneath the range south of the crustal root from a limited number of *Pn* arrivals from two shots. Upper mantle velocities range from 7.99 to 8.12 ±0.20 km/s (Figure 4). The velocity in mantle layer 8 is poorly constrained by transmitted *Pn* arrivals which turn in layer 7. The velocities in this layer range from 7.90 to 8.11 ±0.20 km/s.

The near-offset to wide-angle *PmP* phases from four shots sampling the crustal root zone show a prominent double event (Figures 2, 3d, 4a, and 7a). We have modeled the shallower event as a *PmP* reflection from the Moho; we interpret the deeper event as a reflection from an interface within the mantle north of the crustal root, shown in the velocity model as the top of layer 7 north of the crustal root. A low-fold CMP section of these reflections made from three near-offset (≤35 km) shots is shown in Figure 7b. This mantle reflection zone is 1.5 to 2.0 s thick, appears to be continuous with the lower crustal reflectivity south of the crustal root, and dips to the north at about 15°. We have modeled the top of the Moho reflectivity as a floating reflector, which lies 4 to 5 km above the top of layer 7. We believe this zone of reflections is a continuation of the reflectivity above the Moho seen dipping into the root zone from the south. We interpret the reflective zone in the mantle as a slab of subducted lower crustal rocks. The geometry suggests a continental subduction zone, in which the lower crust and upper mantle seen south of the crustal root are subducted northward beneath the lithosphere under the Colville basin and North Slope. In this interpretation the base of the reflections represents the Moho of the descending plate. We discuss this more fully below.

## Gravity Models

The Brooks Range and southern Colville basin are characterized by an asymmetric gravity low while the southern Brooks Range and Yukon-Koyukuk basin are characterized by a gravity high [*Nunn et al.*, 1987; *Grantz et al.*, 1991] (Figure 8). This positive-negative gravity couple is characteristic of many orogens. The negative anomalies correspond to anomalously thick regions of crust that are associated with the deflection of the crust-mantle boundary or crustal roots. The positive anomalies are typically generated from the subsurface loading of allochthonous material, such as obduction of oceanic crust [*Karner and Watts*, 1983]. In the Brooks Range, minimum gravity anomalies are recorded beneath the EMA (-161 mGal, 265 KM) and maximum anomalies beneath the Angayucham terrane and Yukon-Koyukuk basin (2

mGal, 175 KM). Previous work has characterized the anomalies as resulting from flexural loading of the Arctic Alaskan crust from sediment infill and obduction of crustal blocks to the south [*Nunn et al.*, 1987; *Hawk*, 1985]; and from a southward vergence of subducted slabs beneath a rifted fragment of North America [*Grantz et al.*, 1991]. These studies did not have seismic reflection/refraction data available to constrain the subsurface geometry.

The seismic velocity model described above was used to model gravity data recorded along the trend of the seismic experiment [*Grantz et al.*, 1991; *B. Morin and J. Cady*, unpublished data, personal communication, 1995] (Figure 8). The gravity data were sampled at 5 km intervals along the Dalton Highway, the route of the seismic experiment (148°-151° west longitude, 65°-70° north latitude). Gravity values were reduced with a density of 2.67 g/cm$^3$. The complete Bouguer gravity values are accurate to 0.1 mGal. Gravity anomalies were calculated by holding the boundaries of the velocity model fixed and inverting for density values. Starting density values were obtained from the Nafé-Drake empirical curve [*Ludwig et al.*, 1970]. All final density values resulting from the inversions are within the scatter associated with the data from which the Nafé-Drake relation was derived. The inversions also produced densities which compare well with laboratory measurements of density from hand samples (Tables 2 and 4).

Three gravity models were computed. In the first, the layered velocity model was divided into 16 isodensity polygons, with a uniform density mantle. In the second and third models the zone of reflectivity in the mantle north of the crustal root was assigned a starting density value appropriate for intermediate or mafic lower crustal rocks. In the second model the inverted density in the lower crustal subduction zone was 2.90 g/cm$^3$, a reasonable value for intermediate composition lower crustal rocks (Figure 8b). The geometry of the third model was identical to the second; however, we assumed a gabbroic lower crust which undergoes at least partial phase transition to eclogite as it subducts (Figure 8c). This model produced a subduction layer density of 3.20 g/cm$^3$, not appreciably different from the mantle density in layers 7 and 8 (3.31-3.40 g/cm$^3$). The asymmetry of the gravity minimum is largely controlled by the geometry of the crust-mantle boundary and to a lesser degree by the Doonerak duplex. The inversions are relatively insensitive to the density in the subduction layer.

## Discussion

We have presented seismic velocity and gravity models which are consistent with each other, and with the seismic reflection images of the Brooks Range. Although the velocity model consists of layers in which different elements of a layer correspond to lithotectonic assemblages with different lithologies, metamorphic grades, and/or deformational histories, the velocity parameterization in the layers defined above the basal detachment is dense enough to associate different seismic velocities with different assemblages. We note that direct comparison of laboratory measurements to the average velocities measured in situ is inexact unless the relative volumes of different lithologies in each unit (i.e., velocity probability density functions) are known for the different Brooks Range terranes. In most cases these are not available. In some cases the geologic mapping does not differentiate units having substantially different laboratory velocities. Without a velocity or lithology probability density function, it is difficult to construct an average assemblage velocity from the rock physics data which is meaningful at the scale sampled in the seismic experiment [e.g., *Levander et al.*, 1994; *Rudnick and Fountain*, 1995].

## Whole Crustal Structure

Mean crustal velocity in the Brooks Range is 6.34 ±0.31 km/s, comparable to, but slightly less than, both the worldwide average for continental crust of 6.45 ±0.23 km/s [*Christensen and Mooney*, 1995] and the average for Mesozoic-Cenozoic contractional orogenic belts of 6.39 ±0.15 km/s [*Rudnick and Fountain*, 1995]. Maximum crustal thickness in the Brooks Range is only slightly less than average for similar age mountain belts, being 49 km as compared to 52.4 ±13 [*Rudnick and Fountain*, 1995] and is roughly 25% greater than global averages for continental crust (39 ±8.52 km [*Christensen and Mooney*, 1995]). The velocity depth profiles (Figure 6) as well as the two-dimensional velocity model (Plate 2 and Figure 4a) emphasize the lateral and vertical velocity heterogeneity measured in the crust above the detachment. The steep near surface velocity gradients cause rays to turn at shallow depths relative to the whole crust (above 15 km compared to 49 km). The velocity of the subdetachment crust is close to 6.55 km/s beneath most of the Brooks Range and terranes to the south, decreasing to 6.39 km/s beneath the North Slope. These velocities are consistent with felsic to intermediate composition amphibolite and granulite facies gneisses [*Rudnick and Fountain*, 1995; *Christensen and Mooney*, 1995].

## Doonerak Duplex and Southern Metamorphic Subterranes

The Doonerak duplex is a major crustal feature ~150 km long, 15 km thick, and as deep as 28 km. In our interpretation of the seismic data, its base is coincident with the master detachment over its entire length. Recognition of the master detachment is based largely upon the reflection data; there is little resolvable velocity contrast between the Doonerak duplex and the underlying rocks, i.e., between the base of layer 5 and the top of layer 6. This is not surprising, as these pre-

Mississippian rocks originally formed the basement of the late Paleozoic-early Mesozoic Arctic Alaska passive margin. There are also a number of 5 to 15 km long, south dipping reflections imaged within the Doonerak duplex and modeled as floating reflectors. These reflections are interpreted as faults and shear zones within the duplex. Based on K-Ar and apatite fission track age dating, the duplex is believed to have formed late in the development of the range, with uplift occurring as late as 24 Ma [*O'Sullivan et al.*, 1996; *Blythe et al.*, 1996]. Volumetrically, the Doonerak duplex constitutes ~19% of the total Brooks Range crust and ~37% of the crust above the detachment. As such, it is the largest single structure in the folded belt.

The Skajit allochthon, schist belt, and Rosie Creek allochthon are volumetrically small constituents of the Brooks Range folded belt, together comprising less of the range than the Doonerak duplex. Different balanced cross sections predict different volumes and configurations of schist belt rocks [*Wissinger*, 1995; *Wissinger et al.*, 1997]. The only serious disagreement between the velocity model and the laboratory seismic velocity data occurs in the part of layer 3 interpreted as schist belt rocks. The average velocities from laboratory measurements are lower than those measured in the refraction model. Layer 3 has been well sampled by turning rays, therefore we conclude that (1) the highly anisotropic schist belt rocks have been sampled by the refraction experiment in the fast direction, (2) the lab samples from the schist belt do not adequately represent schist belt rocks, or (3) our interpretation of schist belts rocks comprising layer 3 is incorrect. We feel that any of these scenarios is equally likely.

## Subdetachment Crust And Mantle

The crust below the master detachment is relatively transparent to depths of 4 to 9 km above the Moho. In contrast, the lowermost 4-5 km of the crust are highly reflective across the entire range south of the crustal root. The lower 8-9 km of the crust are highly reflective north of the crustal root. The lower crustal reflectivity exhibits a prominent 5-6 km break at the crustal root beneath the EMA. In our refraction/wide-angle reflection modeling, we used *PmP* phases to determine the average middle and lower crustal velocity and north dipping Moho geometry along the southern two thirds of the profile. In the northern part of the range, *PmP* arrivals were used to constrain the asymmetric geometry of the Moho across the root zone and the structure of the sub-Moho structure.

The upper mantle event aligns well with the north dipping zone of Moho reflections imaged across the southern two thirds of the profile, thus forming a continuous band of reflections that extends 200 km, from 32 km depth beneath the Ruby terrane in the south to ~65 km depth beneath the Colville basin. The constant thickness of the lower crustal reflective zone beneath the range south of the root and in the upper mantle argues that they form a single continuous feature. North of the root zone, this reflective zone is overlain by the shallower south dipping reflections identified as Moho. We interpret the reflections as a "double Moho" beneath the range front (Figures 2, 4, 5i, and 7) resulting from delamination of the lowermost Brooks Range crust and the upper mantle. Seismic images from the Pyrenees and Alps also show show similar Moho offsets in the crustal root zone [*Choukroune*, 1989; *Pfiffner et al.*, 1990; *ETH Working Group*, 1991]; in the Brooks Range the double Moho appears not only as a break in Moho depth, but as two distinct coherent events with different dips, one above the other.

We interpret the reflection geometry as showing that the lower crust and upper mantle to the south of the crustal root were subducted beneath the North Slope crust in an intracontinental setting or behind a continental margin. The reflective zone may then represent either an extremely sheared lower crust and/or a zone of mechanically mixed lower crustal and upper mantle rocks. We have been unable to detect a high-velocity zone at the base of the crust as the angular distribution of rays sampling the lower crust is poor and is biased toward near offsets, making velocity estimates for the lowermost crust difficult. If the intracontinental subduction hypothesis is correct, then in either case the lower crustal reflective zone is acting as a broad shear zone mechanically decoupling the lower crust and upper mantle from the crustal column above it. The reflective zone north of the root zone then likely represents deformation in the wedge of the overriding plate. The gravity and seismic data will permit either inclusion or exclusion of lower crustal rocks in the subduction zone. The age of activity of the subduction zone is unclear. Proximity suggests that subduction could be associated with the uplift and formation of the Doonerak duplex (60-25 Ma), with the formation of the duplex and lower crustal subduction possibly the upper and lower crustal responses to low-angle subduction of the Kula plate. This would remove the implied necessity of relying upon stresses transmitted through the crust over the long distance (~500 km) from the southern Alaska subduction zone to drive the Cretaceous to Cenozoic uplift of the Brooks Range.

Intracontinental subduction has been suggested by Moho asymmetry and migrated near vertical incidence data in the Alps and the Pyrenees [*Holliger*, 1990; *ETH Working Group*, 1991; *Mugnier and Marthelot*, 1991; *Choukroune*, 1989]. The reflective lowermost crust in the Brooks Range is roughly the same thickness as that observed in the Alps and is visually similar in complexity. We believe that the continuity of this zone beneath the North Slope shows the lower crust subducting in an intracontinental subduction zone. The upper mantle reflections appear over approximately 50 km, corresponding to ~250-325 km$^2$ of lower crust in the upper mantle in the profile.

An alternate interpretation of the upper mantle reflections is that they result from a pre-Brookian or Brookian ocean-continent subduction zone. The mantle reflections

seen beneath the Brooks Range could result from the northward subduction of oceanic crust beneath the Brooks Range at ~135 Ma hypothesized by *Blythe et al.* [1996]. Ocean-continent and ocean-island arc paleosubduction zones have been observed in seismic data in continental crust northwest of the British Isles [*Warner et al.,* 1996], in the Gulf of Bothnia [*BABEL Working Group*, 1990], and in the Trans Hudson orogen of the Canadian shield [*Calvert et al.,* 1995]; however, the 4 to 5 km thick complex seismic reflectivity pattern is unlike the reflections seen in other oceanic paleosubduction zones.

## Conclusions

The seismic velocity model for the Brooks Range and surrounding terranes is based upon *Pg*, *PmP*, and limited *Pn* travel time observations from 42 shot points. The principal structures seen in the seismic reflection images were used in the velocity model parameterization to constrain the travel time inversion. The primary constraints utilized from the seismic reflection data are (1) the location of the basal decollement, (2) the base of the EMA at 5-6 km depth, (3) the top of the Doonerak duplex, (4) a north dipping reflector beneath the Yukon-Koyukuk basin which extends to 20 km depth, and (5) the lower crust, Moho, and upper mantle reflections. Seismic velocities in the North Slope sediments, Endicott Mountains allochthon and rocks beneath it, the Doonerak duplex, Skajit allochthon, and elements of the schist belt are well resolved in the inversion. In situ seismic velocities in the Brooks Range above the master decollement are generally in good agreement with laboratory velocities measured in northern Alaska rocks. The Doonerak duplex is the largest structural element above the basal detachment, constituting some 37% of the Brooks Range folded belt. To the west of our seismic line it is exposed in a window through the EMA, beneath our seismic line it extends to depths as great as 28 km. Large-scale thrust structures such as the Doonerak duplex have only recently been imaged seismically at crustal and lithospheric scales [*Price*, 1986; *Green et al.,* 1993; *Cook and Varsek,* 1994, *Levander et al.,* 1994]. Our findings add to a growing body of evidence which links supracrustal detachments in the foreland of a fold and thrust belt to intracrustal and lower crustal detachments in the hinterland by a basal decollement.

Velocities beneath the detachment and the Moho are not well resolved, with errors of ±0.20 km/s. The combination of the wide-angle and near-vertical incidence reflection data, however, provides a clear picture of an asymmetric crustal root extending to 49 km depth beneath the Endicott Mountains allochthon. The vertical-incidence and wide-angle data also provide images of a complex reflective zone directly above the Moho and of a double Moho beneath the northern Brooks Range and southern Colville basin. The northward dipping Moho and lower crustal zone of reflectivity dip continuously from one end of the Brooks Range to the other (75 KM to 325 KM) and continue beneath the shallower southward dipping Moho associated with the North American cratonic rocks underlying the Colville basin and North Slope. The northern, shallower Moho extends from the northern edge of the velocity model (400 KM) to the EMA at 280 KM. The proximity of the lower crustal subduction zone to the recently (25 Ma) uplifted Doonerak duplex suggests that intracontinental subduction may have helped drive upper crustal deformation. Complex reflectivity north of the continental subduction zone is likely the result of deformation of the lower crust and upper mantle of the overriding plate.

## Appendix: Model Resolution

Model parameter resolution is controlled by a number of different factors including experiment geometry, accuracy of travel time picks, model parameterization, diffraction effects which are not considered by ray theory [*Williamson and Worthington*, 1993], the velocity gradients which influence raypaths and effect parameter sampling, and a priori constraints. Isolating the effects of any one of these factors on model resolution is difficult, but once a velocity model has been parameterized, resolution of the model parameters with respect to the data may be statistically determined. Discussion of formal model resolution is given by *Menke* [1984]. The layering chosen for the Brooks Range velocity model was constrained by the reflection image, making independent assessment of the velocity/depth parameters difficult. Here we discuss resolution of the velocities in the crust above the detachment, the only part of the velocity model sampled by turning rays. Figure A1 shows the diagonal of the model resolution matrix obtained from the least squares inversion of *Pg* arrivals for the crust above the detachment (Figures 5a and 5b). The magnitude of each diagonal element indicates the relative degree to which individual model parameters (i.e., velocities) are resolved. Maximum resolution values of 0.6-0.75 are achieved for model parameters located in the center of the model, where ray coverage is most dense (model parameter numbers: 70-93, 125-140), while lower values (0.1-0.3) characterize parameters located on the edges of the model. Where ray coverage is densest, velocities are well resolved from the surface to approximately 20 km depth. Velocity nodes deeper than 30 km are unresolved by the *Pg* phase, since *Pg* rays do not sample these regions and are instead constrained by either *PmP* reflections phases or *Pn* phases. Tests such as those described by *Zelt and Smith* [1992], and *Zelt and White* [1995] indicate that velocity uncertainties are lowest in the upper crust (±0.05 km/s) and highest in the lower crust and upper mantle where little ray coverage is available and gradients are smoother (±0.20 km/s).

**Acknowledgments.** We would like to thank the many people involved in the field work in the Brooks Range, particularly Ed Criley (USGS), Jim Fowler (PASSCAL), Isa Asudeh (Geological Survey of Canada), Stuart Henrys (DSIR, New Zealand), Will Kohler (USGS), Lorraine Wolf (Auburn University), Brad Carr, Chris Humphreys (University of Wyoming), and David Stone (Geophysical Institute of the University of Alaska at Fairbanks). Klaus Holliger (ETH) provided the code for the line drawing depth migrations. Conversations with Colin Zelt (Rice) guided our choices for velocity model parameterization and helped us develop stable models. Bill Symes (Rice) provided a great deal of insight regarding model resolution. Tim Henstock, Steve Larkin, and Colin Zelt provided valuable criticisms of the manuscript. This research has been supported by IRIS Subaward Agreements 0127 and 0140 and NSF grants EAR8905222 and EAR9105002 and by the USGS Deep Crustal Studies Program. The Air Force Geophysics Lab provided additional field support.



## References

BABEL Working Group, Evidence for early Proterozoic plate tectonics from seismic reflection profiles in the Baltic Shield, *Nature, 348*, 34-38, 1990.

Blythe, A.E., J.M. Bird, and G.I. Omar, Deformational history of the central Brooks Range, Alaska: Results from fission-track and 40Ar/39Ar analyses, *Tectonics, 15*, 440-455, 1996.

Box, S.E., and W.W. Patton Jr., Early Cretaceous evolution of the Yukon-Koyukuk basin and its bearing on the development of the Brookian orogenic belt, Alaska, paper presented at the *AAPG-SEPM-SEG Pacific Section Meeting*, 1985.

Calvert, A.J., E.W. Sawyer, W.J. Davis, and J.N. Ludden, Archaean subduction inferred from seismic images of a mantle suture in the Superior Province, *Nature, 375*, 670-674, 1995.

Choukroune, P., The ECORS Pyrenean Deep Seismic Profile Reflection Data and the Overall Structure of an Orogenic Belt, *Tectonics, 8*, 23-39, 1989.

Christensen, N.I., and W.D. Mooney, Seismic velocity structure and composition of the continental crust: A global view, *J. Geophys. Res., 100*, 9761-9788, 1995.

Cook, F.A., and J.L. Varsek, Orogen-scale decollements, *Rev. Geophysics, 32*, 37-60, 1994.

ETH Working Group, Integrated analysis of normal incidence and wide-angle reflection measurements across the eastern Swiss Alps, in *Continental Lithosphere: Deep Seismic Reflections*, Geodyn. Ser., vol. 22, edited by R. Meissner et.al., pp. 195-206, AGU Washington D.C., 1991.

Fuis, G.S., A.R. Levander, W.J. Lutter, E.S. Wissinger, T.E. Moore, and N.I. Christensen, Seismic images of the Brooks Range, Arctic Alaska, reveal crustal scale duplexing, *Geology, 23*, 65-68, 1995.

Gottschalk, R.R., Tectonics of the schist belt metamorphic terane near Wiseman, Alaska, *Geol. Soc. Am. Abstr. Programs, 19*, 383, 1987.

Gottschalk, R.R., Structural evolution of the schist belt, south central Brooks Range fold and thrust belt, Alaska, *J. Struct. Geol., 12*, 453-69, 1990.

Gottschalk, R.R., and J.S. Oldow, Low-angle normal faults in the south-central Brooks Range fold and thrust belt, Alaska, *Geology, 16*, 395-99, 1988.

Grantz, A., T.E. Moore, and S.M. Roeske, North American Continent-Ocean transect A-3: Gulf of Alaska to Arctic Ocean, G.S.A. Continental/Ocean Transect A-3, 2 pp., *Geol. Soc. of Am.*, Boulder, Colo., 1991.

Green, A.G., L. Levator, P. Valasek, R. Olivier, St. Mueller, B. Milkereit, and J.J. Wagner, Characteristic reflection patterns in the southeast Canadian Cordillera, Northern Appalachians, and Swiss Alps, *Tectonophysics, 219*, 71-91, 1993.

Hawk, J.M., Lithospheric flexure, overthrust timing, and stratigraphic modeling of the central Brooks Range and Colville Basin, M.S. thesis, 179 pp., Rice Univ., Houston, Tex., 1985.

Holliger, K., A composite, depth-migrated deep seismic reflection section along the Alpine segment of the EGT dervied from the NFP20 eastern and southern traverses, in *The European Geotraverse: Integrative Studies*, edited by R. Freeman, P. Giese, and St. Mueller, pp. 245-254, Eur. Sci. Found., Strasbourg, France, 1990.

Holliger, K., and E. Kissling, Ray theoretical depth migration: methodology and application to deep seismic reflection data across the eastern and southern Swiss Alps, *Eclogae Geol. Helv., 84*, 369-402, 1991.

Jones, D.L., N.J. Silberling, P.J. Coney, and G. Plafker, Lithotectonic terrane map of Alaska, scale 1:2,500,000, *U.S. Geol. Surv. Misc. Field Stud. Maps, MF-1874A*, 1987.

Karner, G.D, and A.B. Watts, Gravity anomalies and flexure of the lithosphere at mountain ranges, *J. Geophys. Res, 88*, 10449-10477, 1983.

Lafond, C.F., A.R. Levander, B.C. Beaudoin, G.S. Fuis, R.A. Page, and D.B. Stone, PASSCAL seismic reflection wave tests in the Brooks Range, Arctic Alaska, *Eos Trans. AGU, 69*, 1453, 1988.

Levander, A., G.S. Fuis, E.S. Wissinger, W.J. Lutter, J.S. Oldow, and T.E. Moore, Seismic images of the Brooks Range fold and thrust belt, Arctic Alaska, from an integrated seismic reflection/refraction experiment, *Tectonophysics, 232*, 13-31, 1994.

Ludwig, W.J., J.E. Nafe, and C.L. Drake, Seismic refraction, in *The Sea*, vol. 4, part 1, edited by A.E. Maxwell, pp. 53-84, Wiley-Interscience, New York, 1970.

Menke, W., *Geophysical Data Analysis: Discrete Inverse Theory*, 260 pp., Academic, San Diego, Calif., 1984.

Miller, E.L., and T.L. Hudson, Mid-Cretaceous extensional fragmentation of a Jurassic-early Cretaceous compres-

sional orogen, Alaska, *Tectonics, 10*, 781-796, 1991.

Moore, T.E., and C.G. Mull, Geology of the Brooks Range and North Slope, in *Alaskan Geological and Geophysical Transect, Field Trip Guide.,* vol. T104, edited by W.J. Nokleberg and M.A. Fisher, pp. 107-131, 1989.

Moore, T.E., W.K. Wallace, K.J. Bird, S.M. Karl, C.G. Mull, and J.T. Dillon, Geology of northern Alaska, *U.S. Geol. Surv. Open File Rep. 92-220*, 191 pp., 1992.

Moore, T.E., W.K. Wallace, K.J. Bird, S.M. Karl, C.G. Mull, C.G., and J.T. Dillon, Geology of northern Alaska, in *The Geology of North America,* vol. G-1, *The Geology of Alaska*, edited by G. Plafker, and H.C. Berg, pp. 49-140 Geol., Soc., Am., Boulder, Colo. 1994.

Mugnier, J.-L., and J.-M. Marthelot, Crustal reflection beneath the Alps and Alpine foreland: Geodynamic implications, *Continental Lithosphere: Deep Seismic Reflections, Geodyn. Ser.,* vol. 22, edited by R. Meissner et al., pp. 177-184, Washington, D.C., 1991.

Mull, C.G., The tectonic evolution and structural style of the Brooks Range, Alaska: An illustrated summary, in *Geological Studies of the Cordilleran Thrust Belt*, vol. 1, edited by R.B. Blake, pp. 1-45, Rocky Mt. Assoc. of Geol., Denver, Colo., 1982.

J.M. Murphy, G.S. Fuis, A.R. Levander, W.J. Lutter, E.C. Criley, S.A. Henrys, I. Asudeh, and J.C. Fowler, Data report for the 1990 seismic reflection/refraction experiment in the Brooks Range, Arctic Alaska, *U.S. Geol. Surv. Open File Rep. 93-265*, 1993.

Nunn, J.A., M. Czerniak, and R.H. Pilger, Constraints on the structure of the Brooks Range/Colville basin, northern Alaska, *Tectonics, 5,* 603-618, 1987.

Oldow, J.S., C.M. Seidensticker, J.C. Phelps, F.E. Julian, R.R. Gottschalk, K.W. Boler, J.W. Handschy, and H.G. Avé Lallemant, Balanced cross sections through the Central Brooks Range and North Slope, Arctic Alaska, Tulsa, Oklahoma, *AAPG Spec. Publ.*. 19 pp., 8 plates, 1987.

O'Sullivan, P.B., T.E. Moore, and J.M. Murphy, Tertiary uplift of the Mt. Doonerak antiform, central Brooks Range, Alaska: Apatite fission evidence from the Trans-Alaska Crustal Transect, *Mem. Geol. Soc. Am.*, 1996.

Pfiffner, O.A., W. Frei, P. Valasek, M. Stauble, L. Levato, L. Dubois, S. Schmid, and S. Smithson, Crustal shortening in the alpine orogen: Results from deep seismic reflection profiling in the eastern Swiss Alps, line NFP20 EAST, *Tectonics, 9,* 1327-1355, 1990.

Price, R.A., The southeastern Canadian Cordillera: Thrust faulting, tectonic wedging, and delamination of the lithosphere, *J. Struct. Geol., 8*, 239-254, 1986.

Raynaud, B., A 2-D, ray-based, depth migration method for deep seismic reflections, *Geophys. J., 93,* 163-171, 1988.

Rudnick, R.L., and D.M. Fountain, Nature and composition of the continental crust: A lower crustal perspective, *Rev. Geophys., 33,* 267-309, 1995.

Stone, D.B., R.A. Page, and J.N. Davies, (eds.), Trans-Alaska lithosphere investigation-Program prospectus, *U.S. Geol. Surv. Circ.*, 984, 24 pp., 1986.

Till, A.B., S.E. Box, S.M. Roeske, W.W. Patton Jr., E.L. Miller, and T.L. Hudson, Comment on "Mid-Cretaceous extensional fragmentation of a Jurassic-Early Cretaceous compressional orogen, Alaska" by E.L. Miller and T.L. Hudson, *Tectonics, 12*, 1076-1086, 1993.

Wallace, W.K., and C.L. Hanks, Structural provinces of the northeastern Brooks Range, Arcic National Wildlife Refuge, Alaska, *AAPG Bull., 74*, 1100-1118, 1990.

Warner, M., J. Morgan, P. Barton, C. Price, and K. Jones, Seismic reflections from the mantle represent relict subduction zones within the continental lithosphere, *Geology, 24,* 39-42, 1996.

Williamson, P.R., and M.H. Worthington, Resolution limits in ray tomography due to wave beahvior: Numerical experiments, *Geophysics, 58*, 727-735, 1993.

Wissinger, E.S., Seismic profiling constraints on the evolution of the Brooks Range, Arctic Alaska, from an integrated reflection/refraction profile, Ph.D. thesis, 325 pp., Rice Univ., Houston, Tex., 1995.

Wissinger, E.S., J.S. Oldow, and A. Levander, Seismic profiling constraints on the evolution of the central Brooks Range, Arctic Alaska, *Mem. Geol. Soc. Am.,* Chapter 11, 1997.

Zelt, C.A. and D.A. Forsythe, Modeling wide-angle seismic data for crustal structure: Southeastern Grenville Province, *J. Geophys. Res, 99*, 11687-11704, 1994.

Zelt, C.A., and R.B. Smith, Seismic travel time inversion for 2-D crustal velocity structure, *Geophys. J. Int., 108*, 16-34, 1992.

Zelt, C.A., and D.J. White, Crustal structure and tectonics of the southeastern Canadian Cordillera, *J. Geophys. Res., 100*, 24255-24,273, 1995.

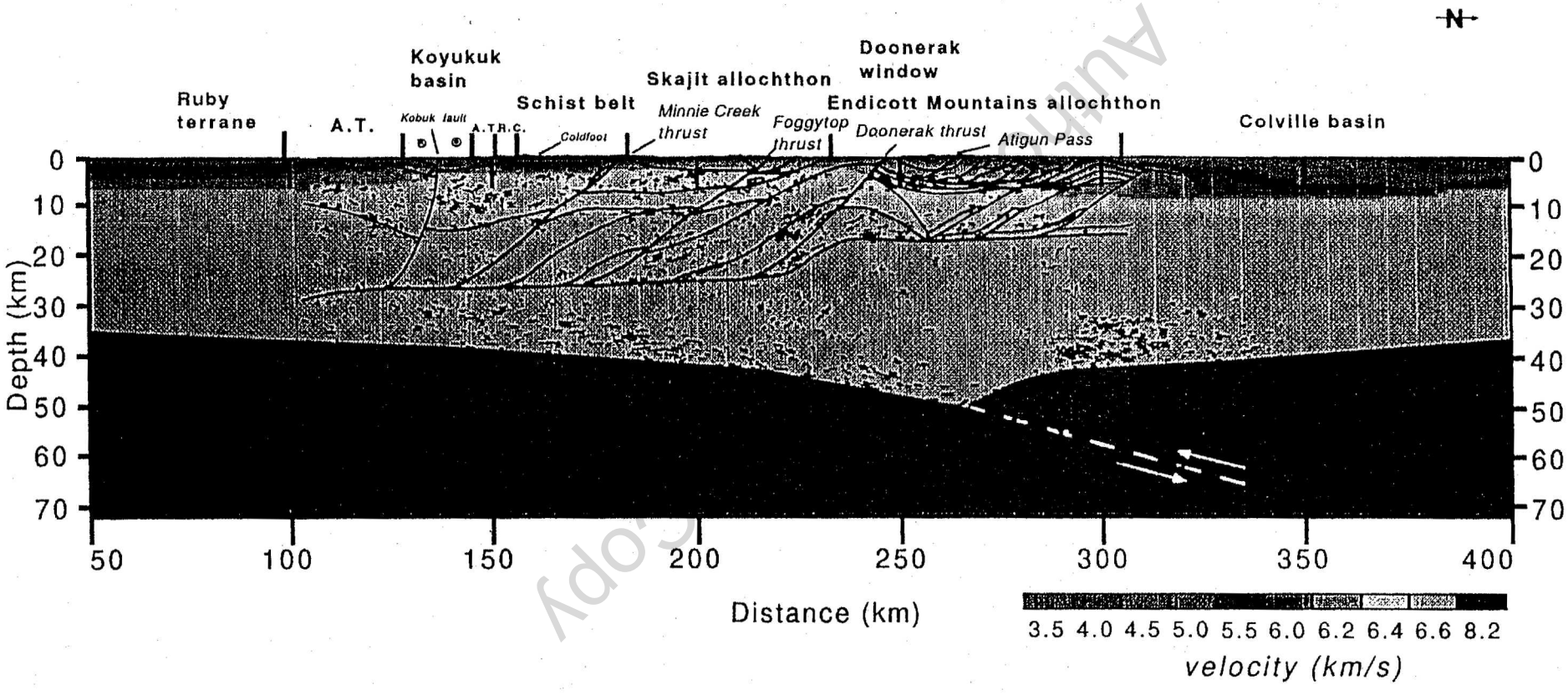


**Plate 1.** Balanced cross section [from *Wissinger*, 1995] and line drawing migration of reflectivity superimposed on the seismic velocity model described in this paper (see Plate 2).

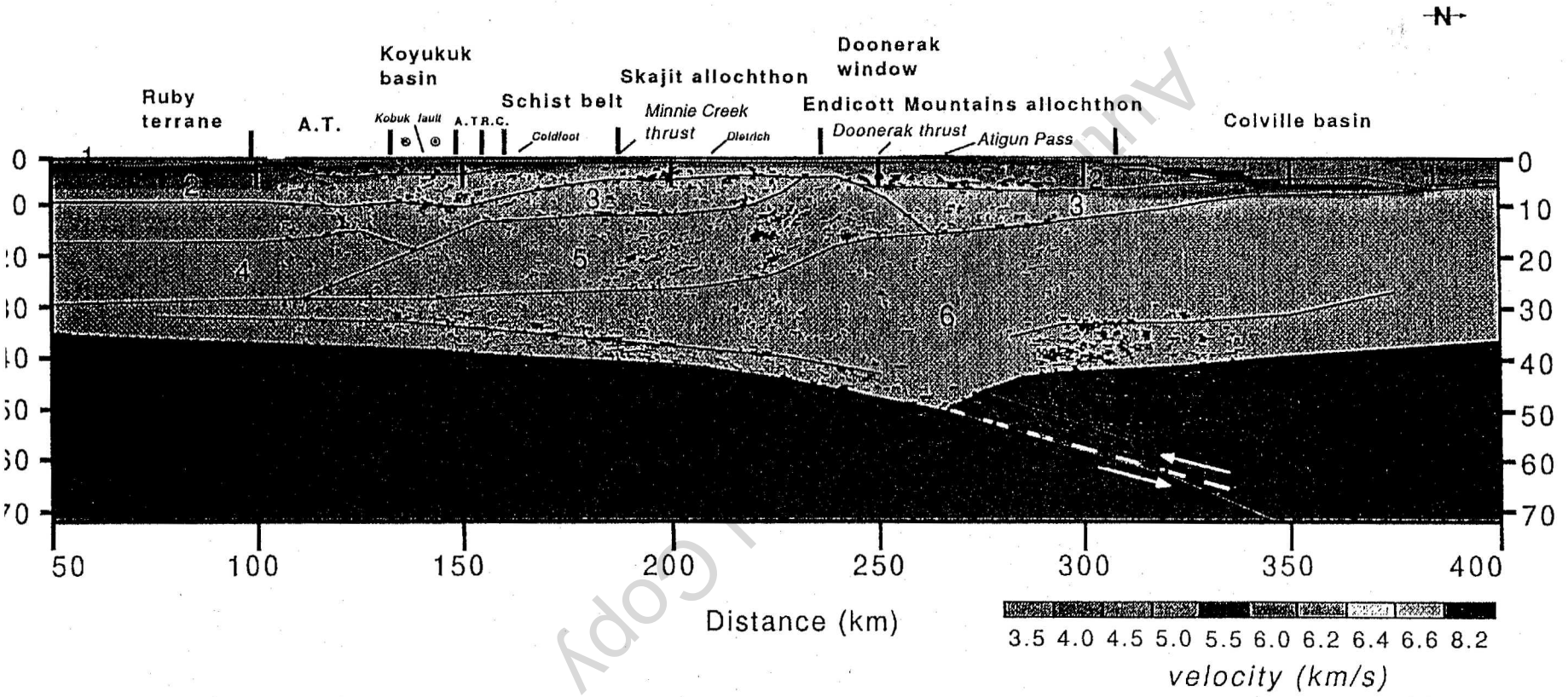


**Plate 2.** Velocity model of the Brooks Range with layer boundaries superimposed, as well as the migrated reflectivity patterns. Layers are numbered as in text.

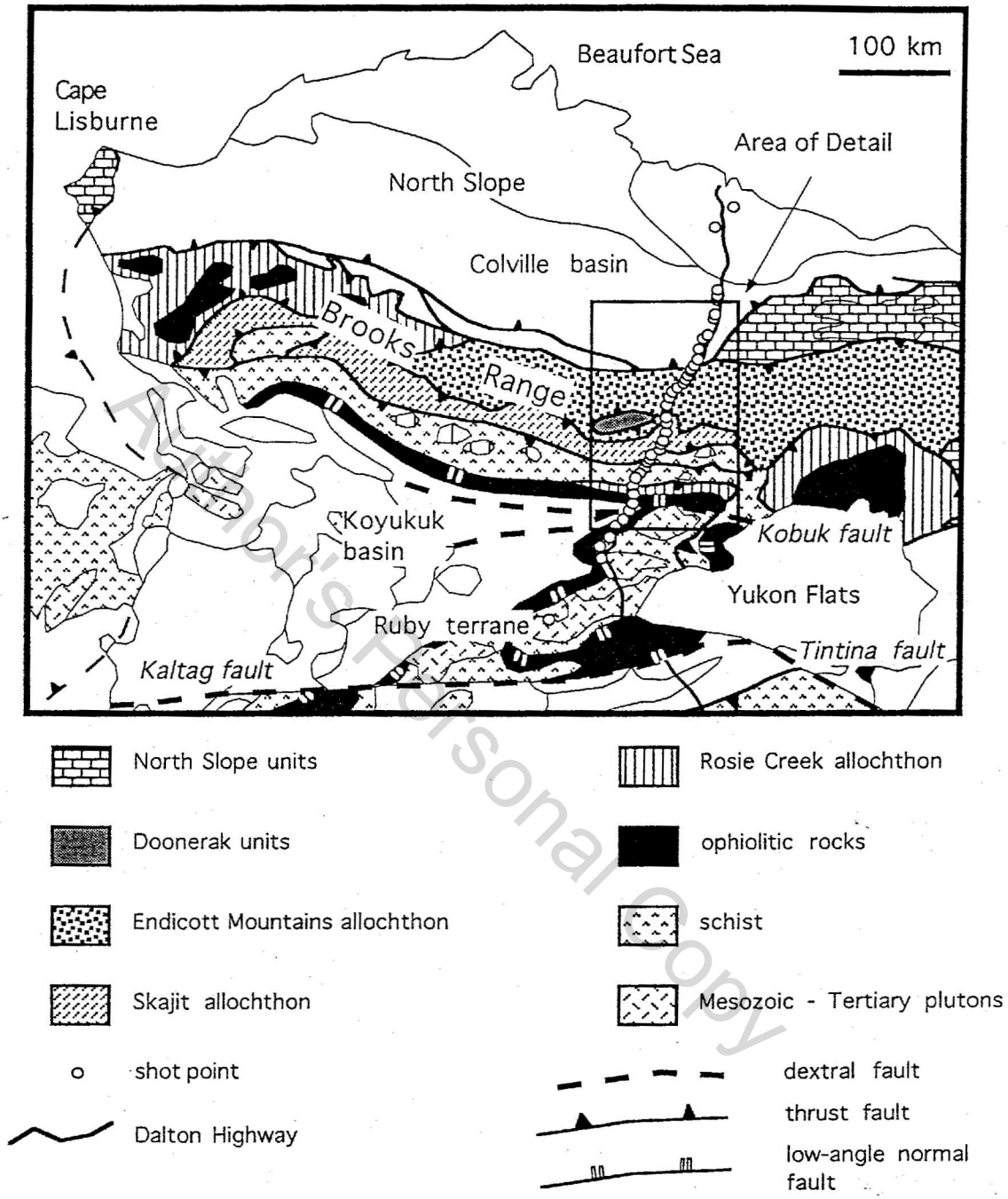




**Figure 1.** Location map for the Brooks Range seismic survey in northern Alaska. The box on the geologic map indicates the extent of the seismic profile described in this paper.

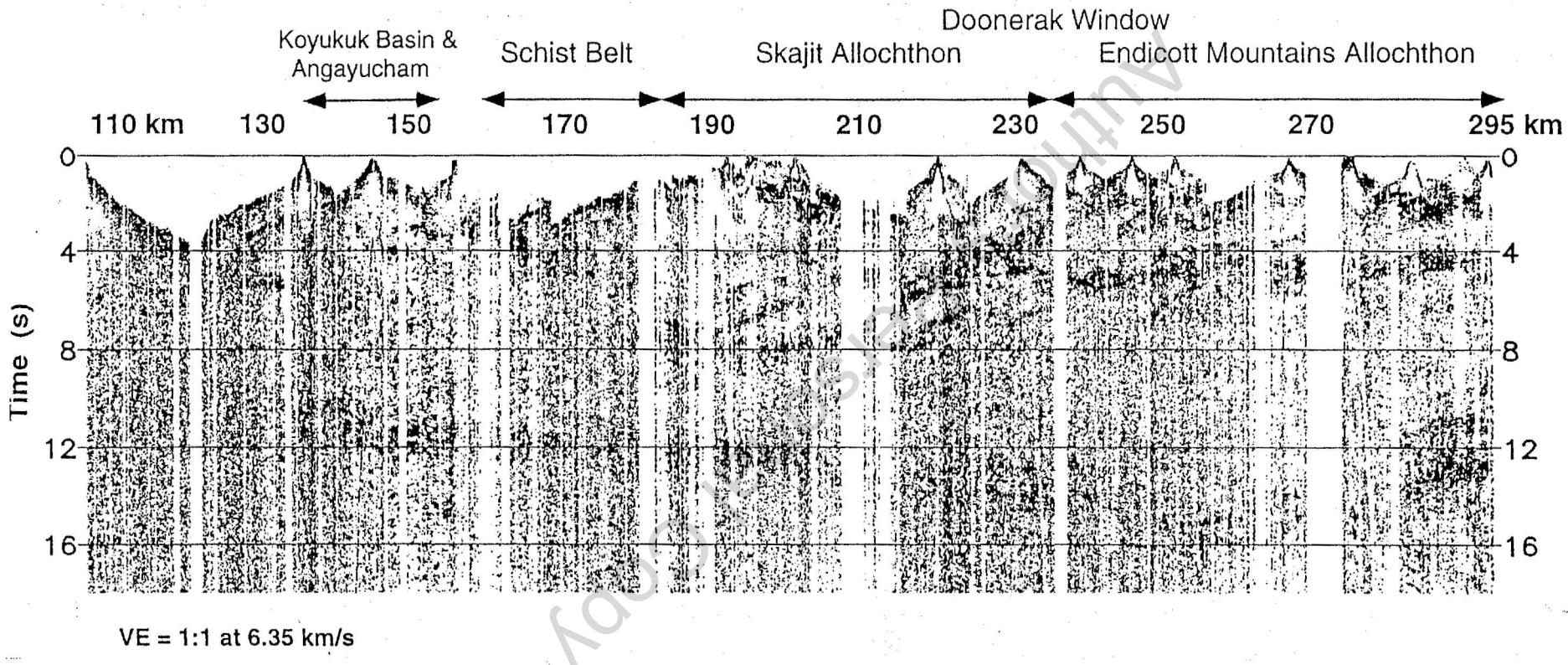


**Figure 2.** Low-fold seismic reflection section across the Brooks Range. The CMP section, made with offsets < 32 km, shows 18 s of data in an energy display. Coordinates on this and all subsequent figures are given in kilometers north of the Arctic Circle.

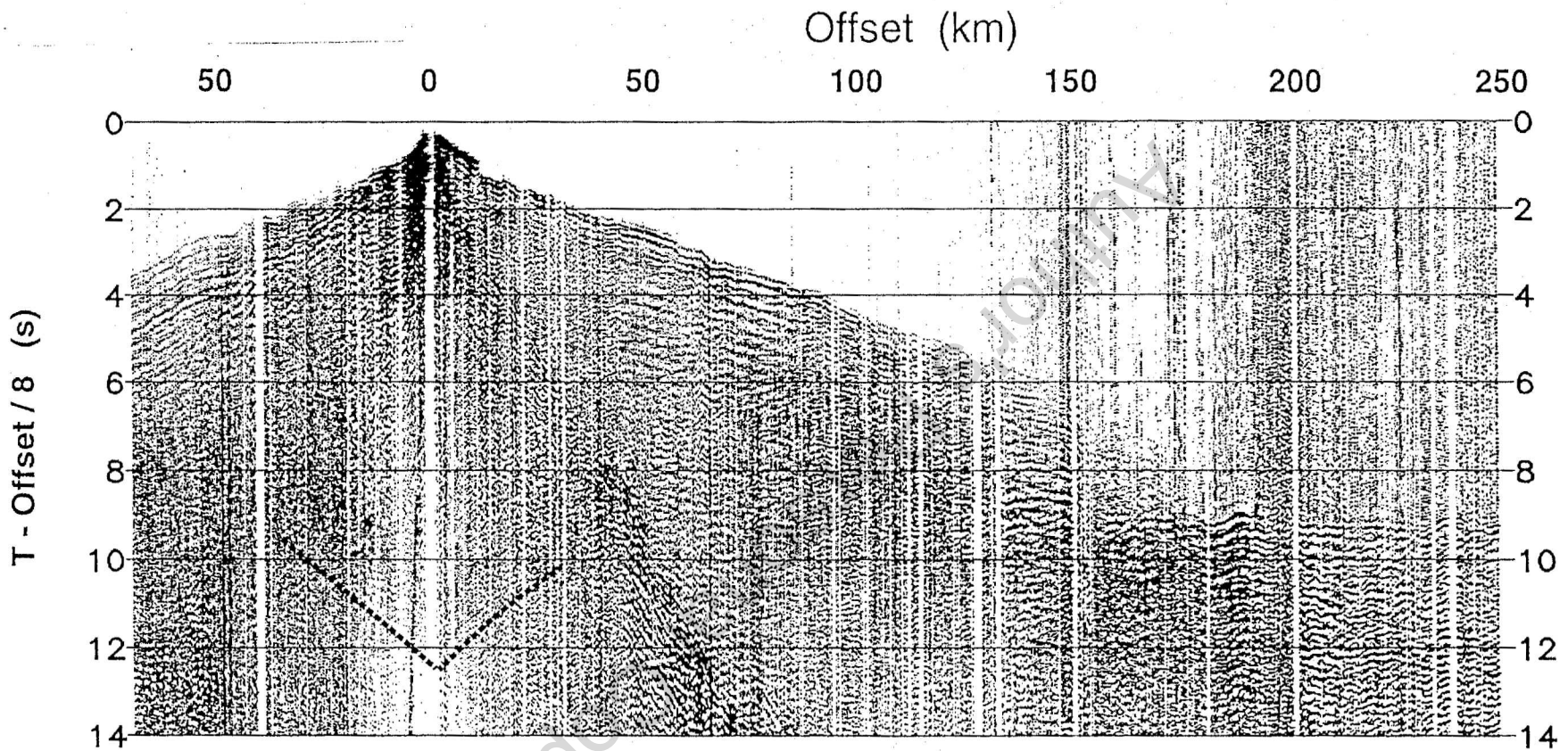


**Figure 3a.** Shot gathers from shot points 126 and 140 showing near and far offset data acquired during the Brooks Range seismic survey. Reduced time record section from shot point 126, at model coordinate 148 KM, shows precritical *PmP* near zero-offset at 12 s (dashed lines), postcritical *PmP* at offsets greater than ~125 km, and *Pn* from 160 to 250 km.

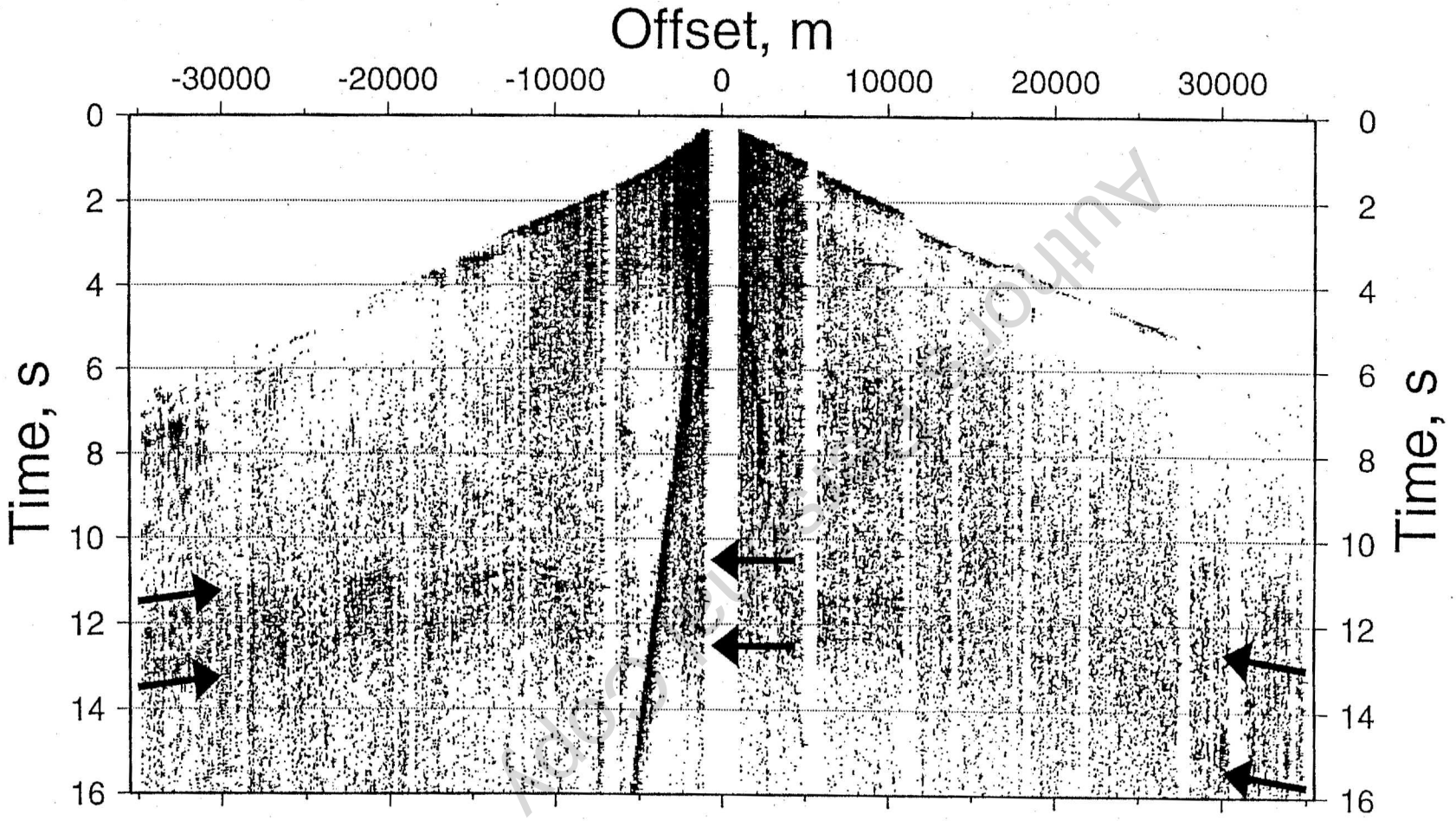


**Figure 3b.** Same record as in Figure 3a in two-way-time at near offsets showing the band of lower crustal and Moho reflectivity.

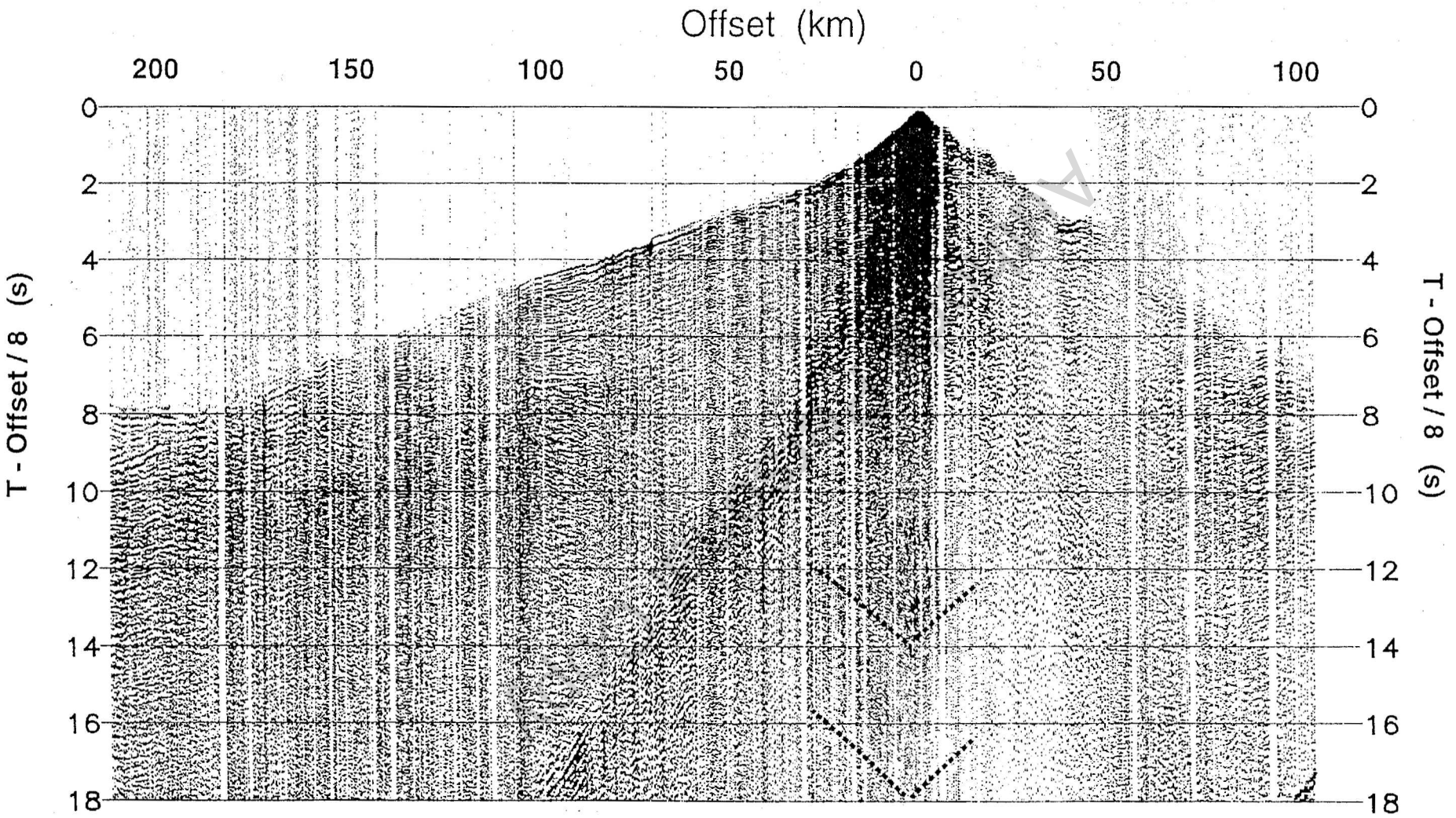


**Figure 3c.** Shot point 140, at model coordinate 292 KM, shows precritical *PmP* near zero-offset at 12 s, postcritical *PmP* at offsets greater than ~125 km, and *Pn* from 180 to 212 km to the south (left).

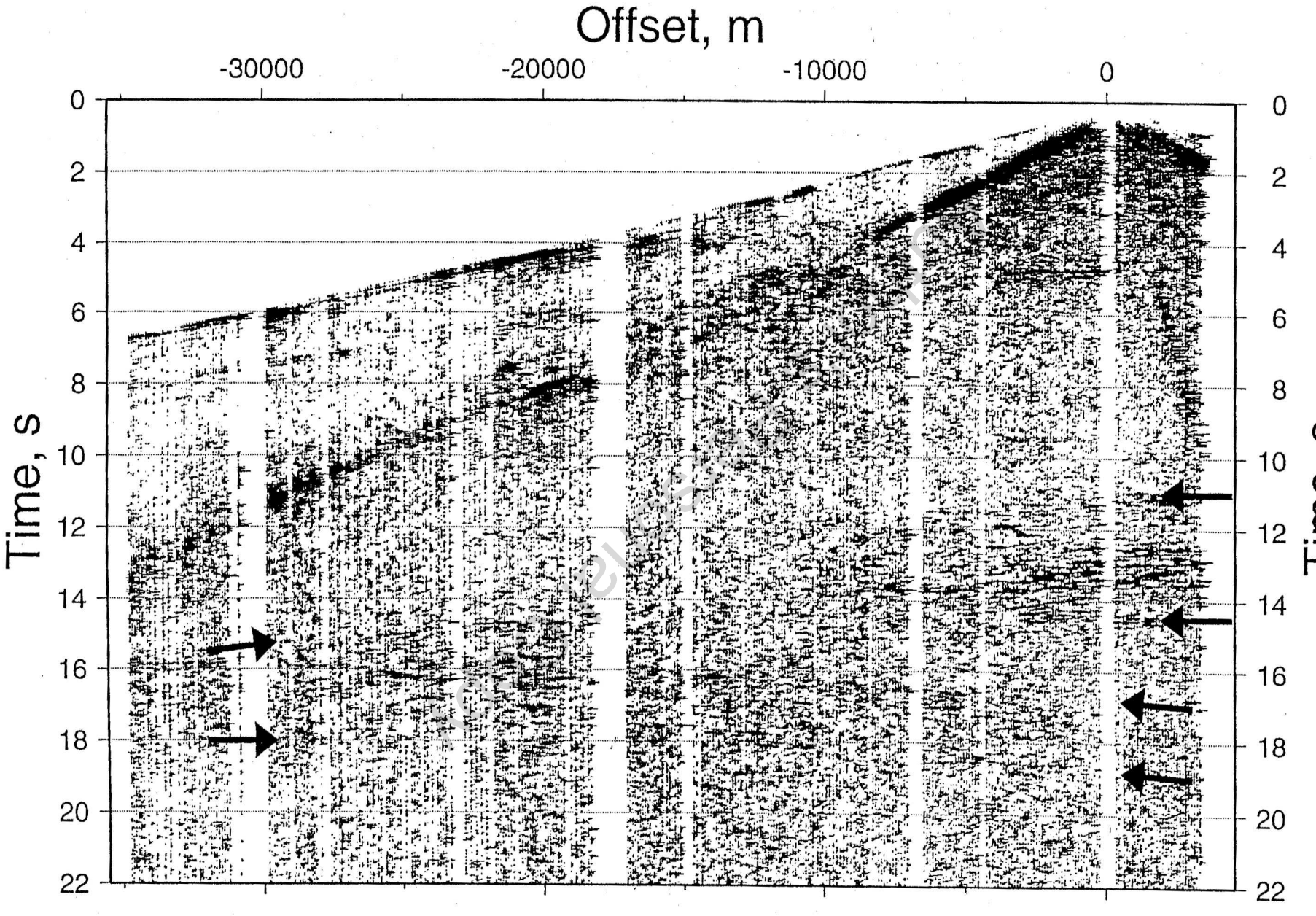


**Figure 3d.** Deep reflections from shot point 140 appear in two zones from 11-14.5 s and 17-19 s near zero-offset. These events have different dips and are clearly separated in different bands.

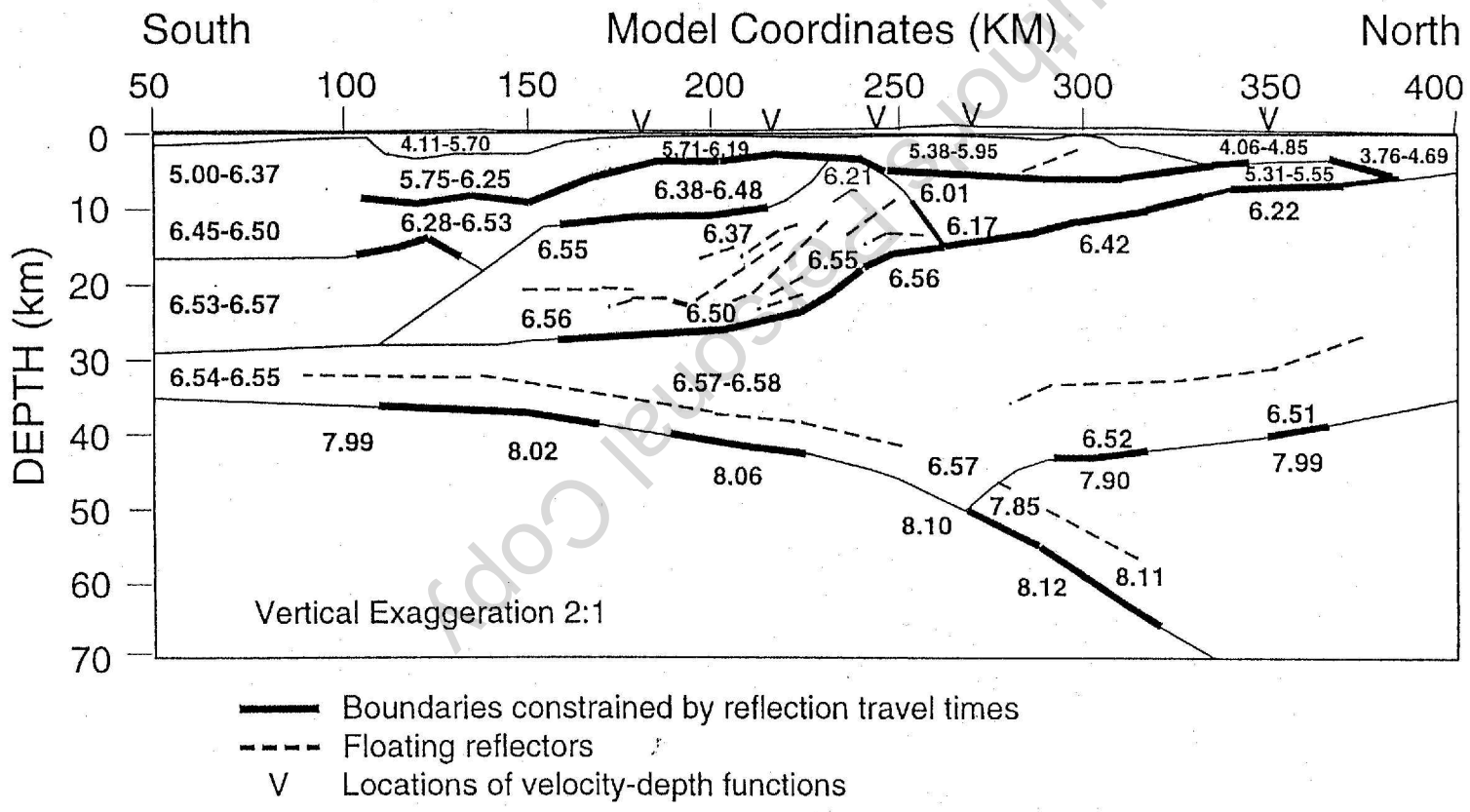




**Figure 4a.** Velocity model of the Brooks Range with velocities determined from the travel time inversion within individual layers shown. Dark lines indicate layer boundaries constrained in the inversion by reflection travel times. Vertical arrows show the location of the velocity depth profiles show in Figure 6. The model is shown with 2:1 vertical exaggeration.

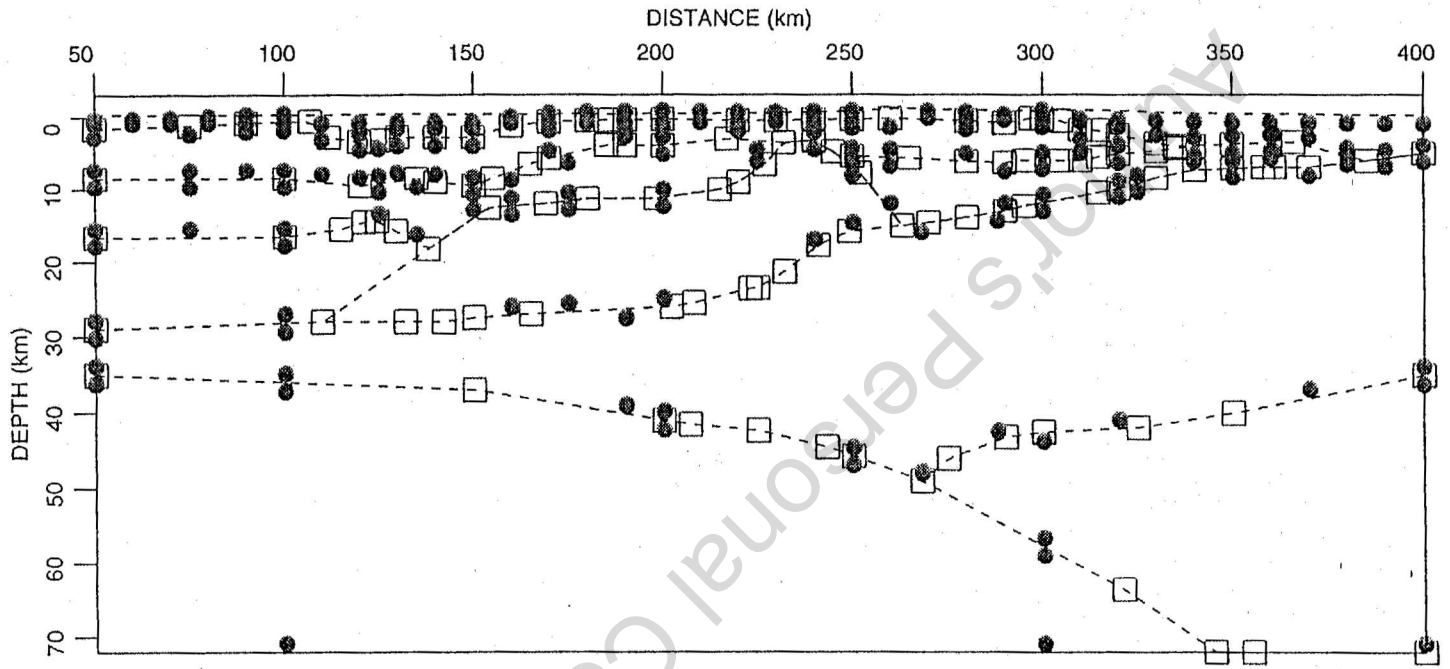




**Figure 4b.** Velocity nodes (shaded circles) and depth nodes (squares) used for the seismic inversion. The model is shown with 2:1 vertical exaggeration.

Figure 5a.

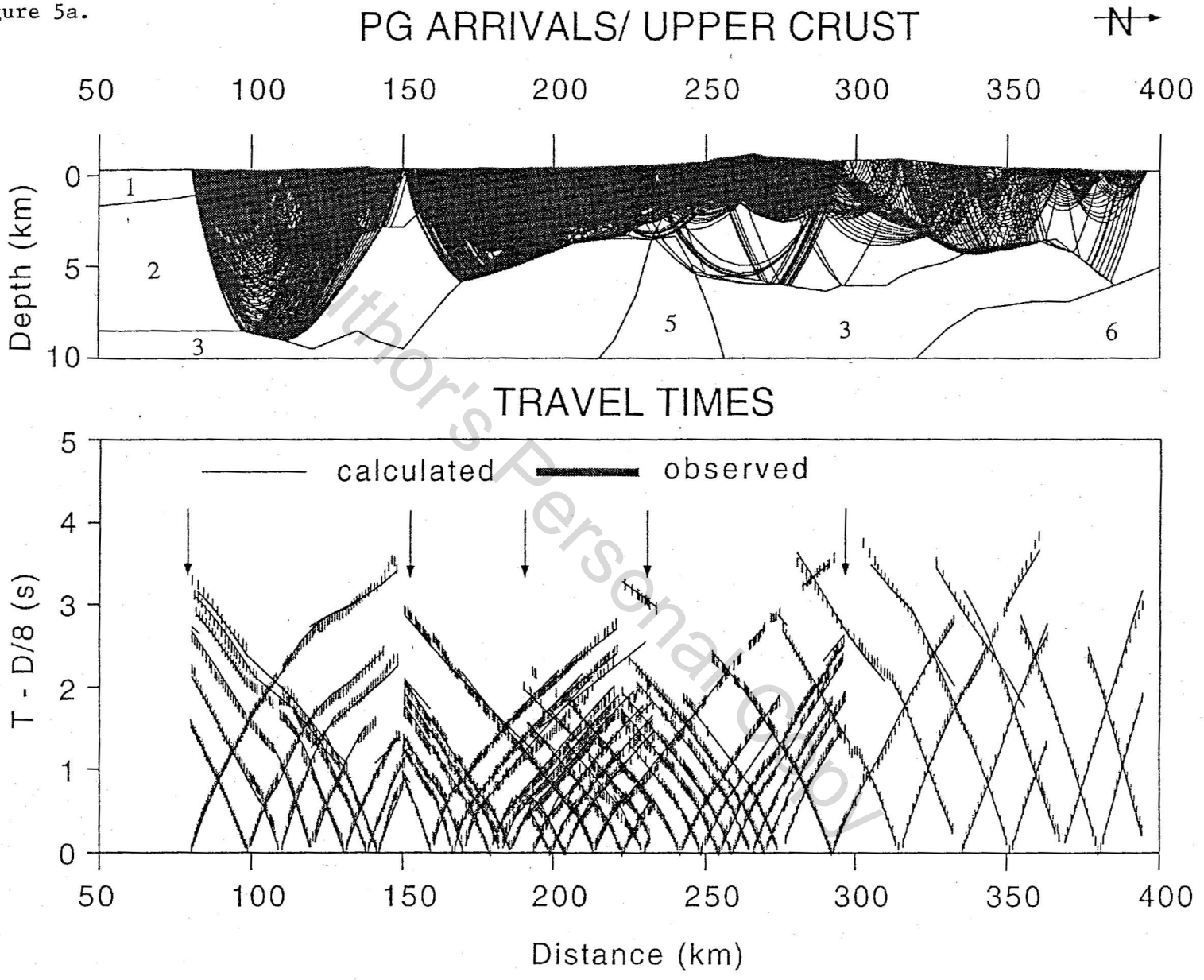




**Figure 5.** Ray diagrams and travel time fits for different layers. (a) and (b) *Pg* arrivals in layers 1-5. (c) Reflections from the base of layer 1. (d) Reflections from the base of layer 2. (e) Reflections from the base of layers 3 and 4. (f) Reflections from the base of layer 5. (g) Floating reflectors in layers 5 and 6. (h) *Pn* and *PmP* arrivals. (i) Floating reflectors in the lower crust and upper mantle.

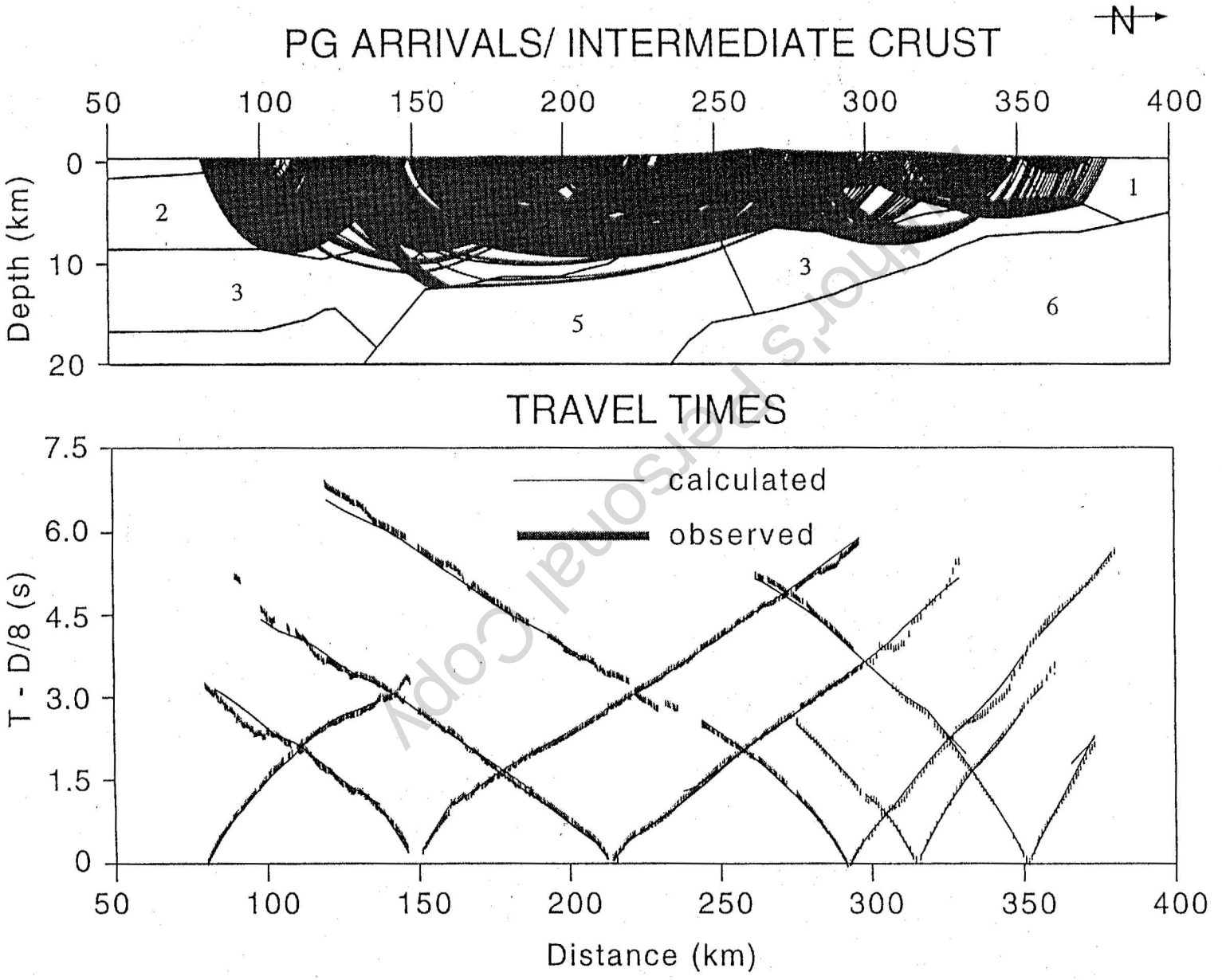
PG ARRIVALS/ INTERMEDIATE CRUST
N
50
100
150
200
250
300
350
400
0
10
20
Depth (km)
1
2
3
3
5
6
TRAVEL TIMES
calculated
observed
7.5
6.0
4.5
3.0
1.5
0
T - D/8 (s)
50
100
150
200
250
300
350
400
Distance (km)

Figure 5b.

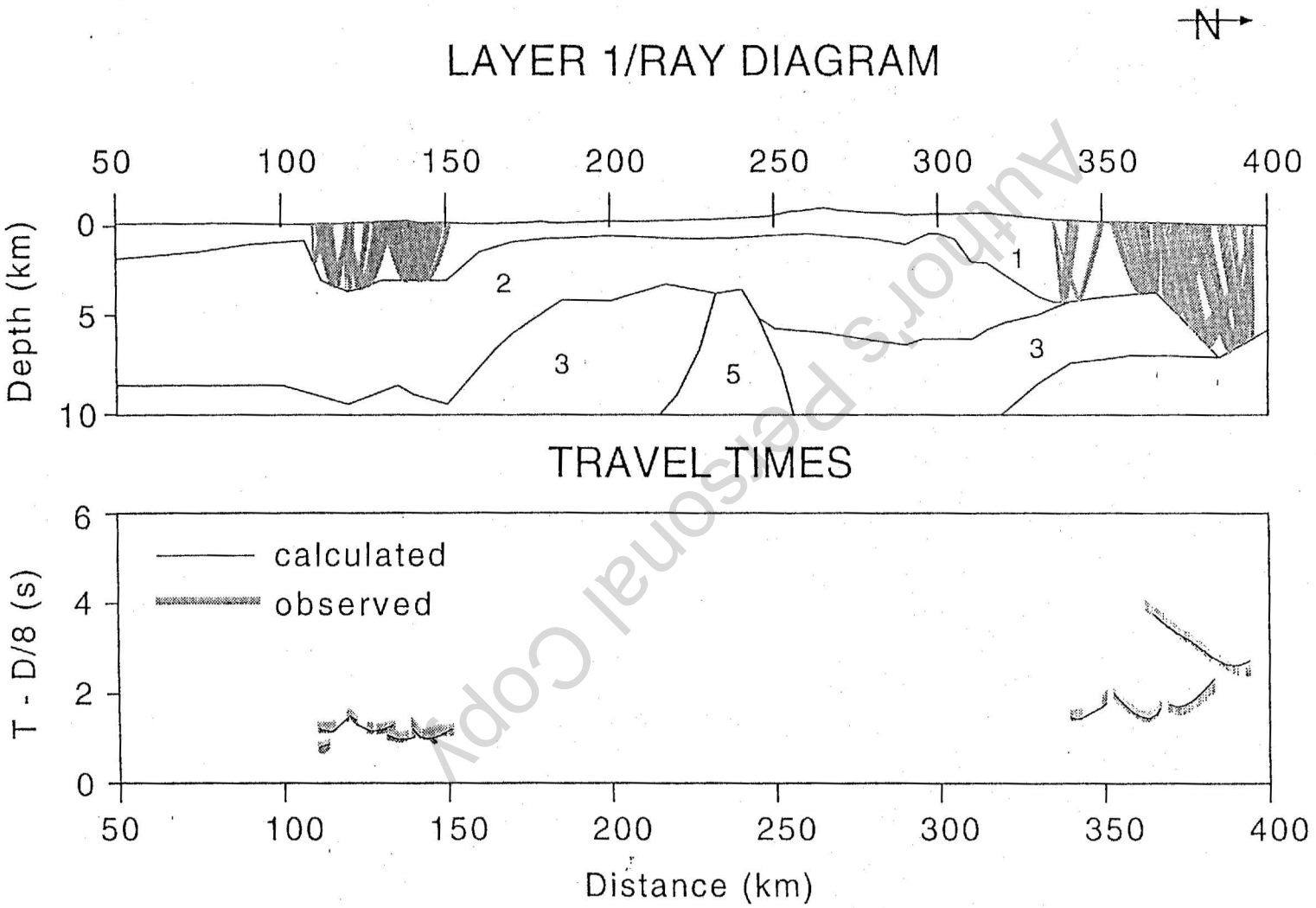




Figure 5c.

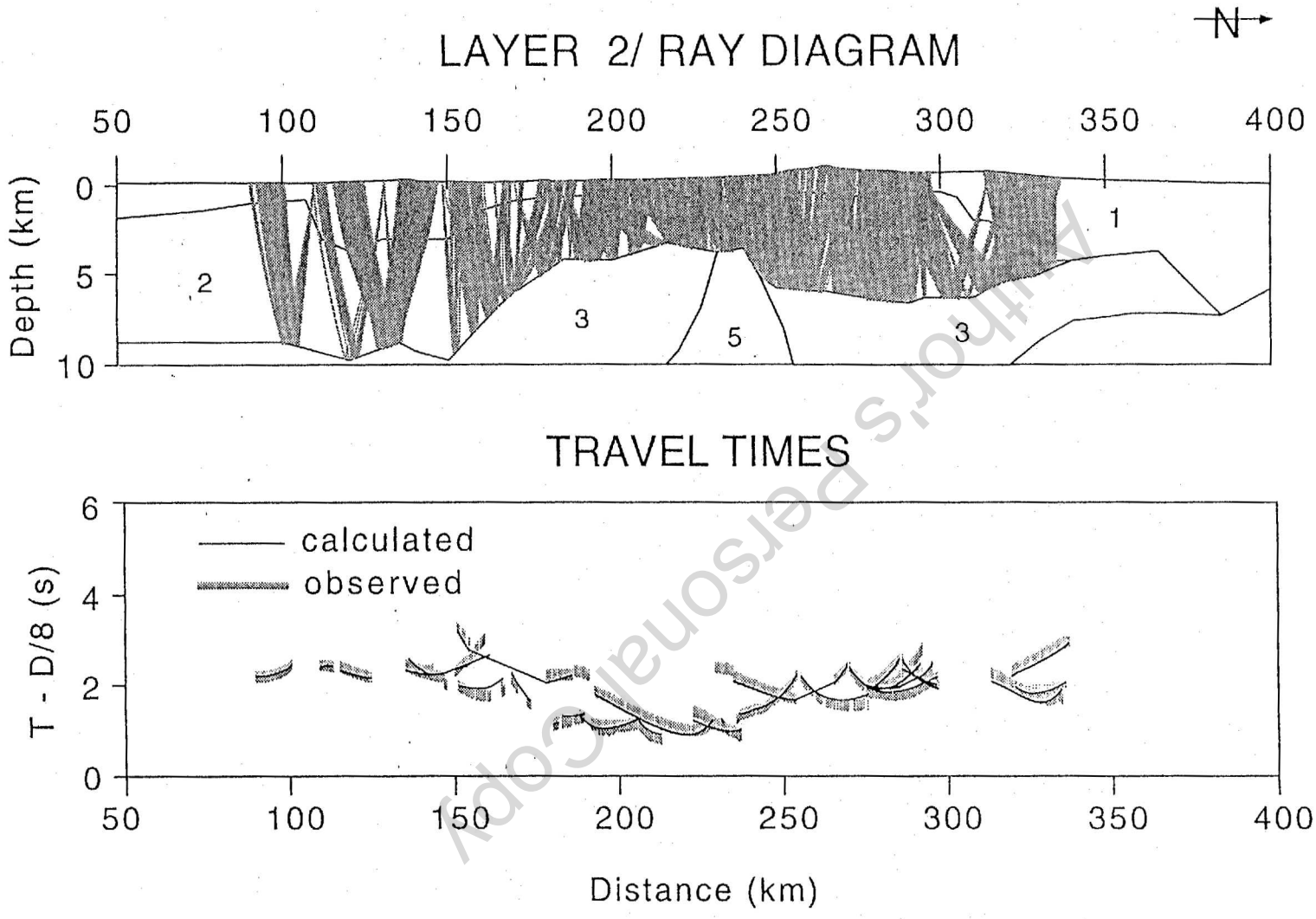




Figure 5d.

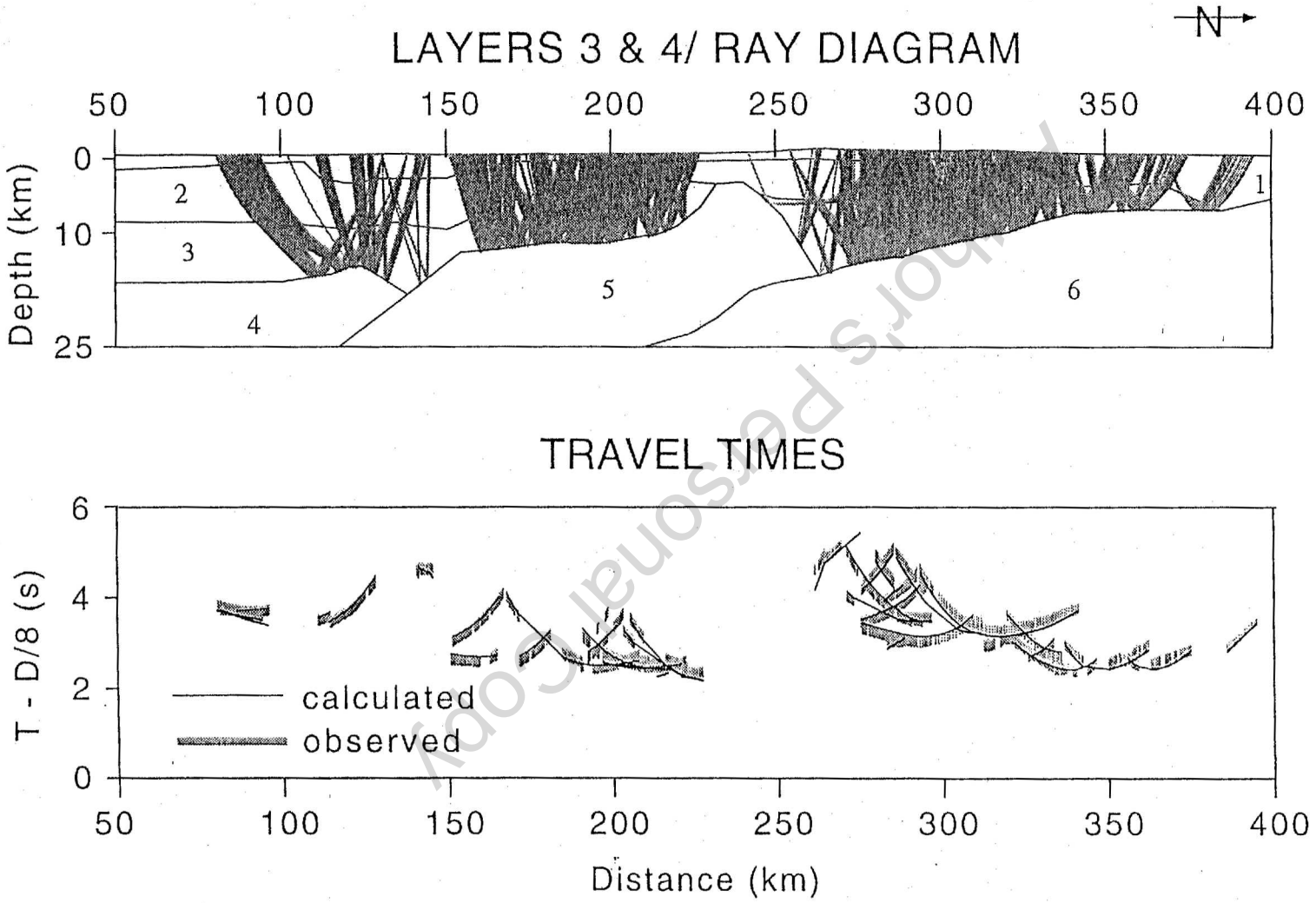
LAYERS 3 & 4/ RAY DIAGRAM
N
50
100
150
200
250
300
350
400
0
10
25
Depth (km)
1
2
3
4
5
6
TRAVEL TIMES
6
4
2
0
T - D/8 (s)
calculated
observed
50
100
150
200
250
300
350
400
Distance (km)

Figure 5e.

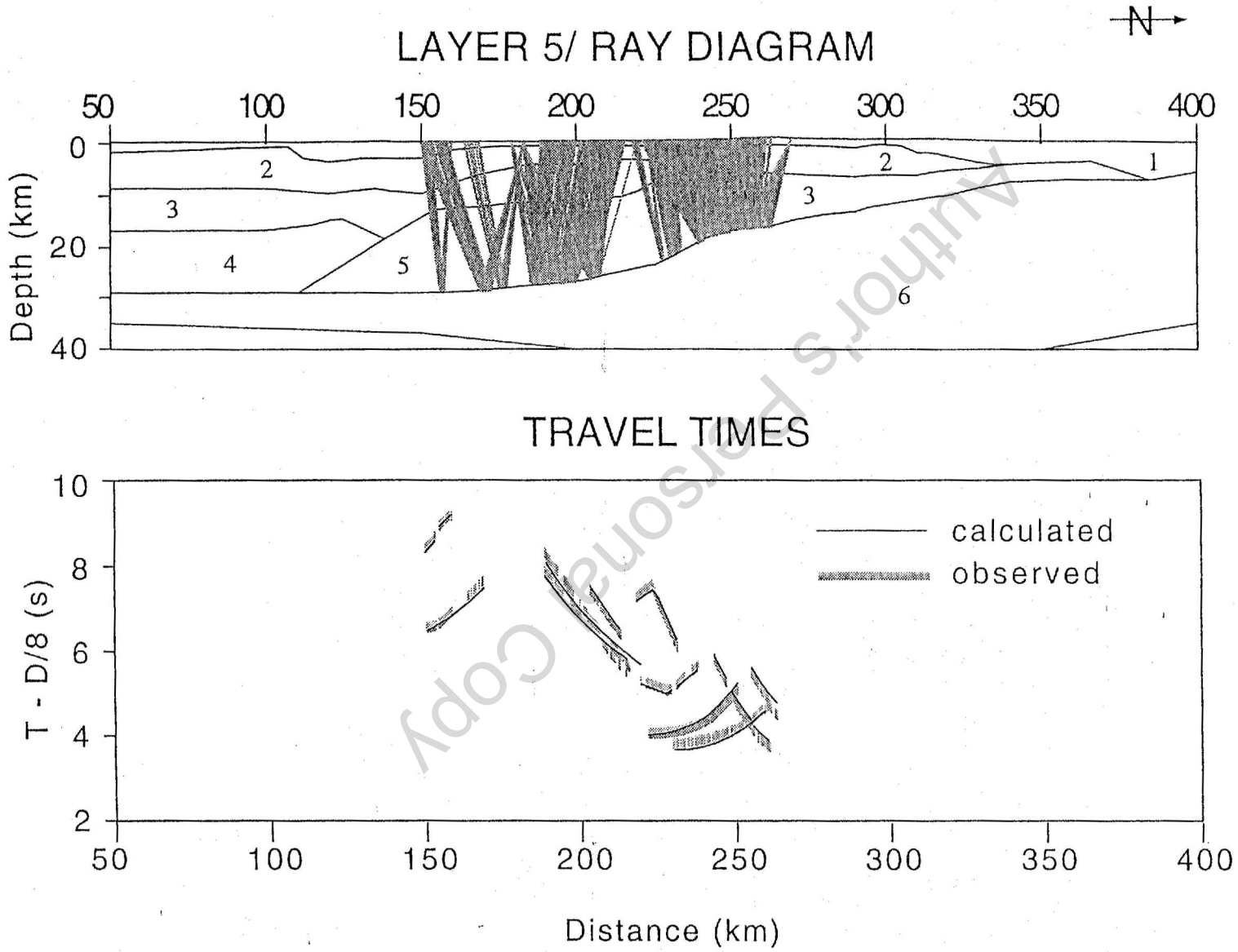




Figure 5f.

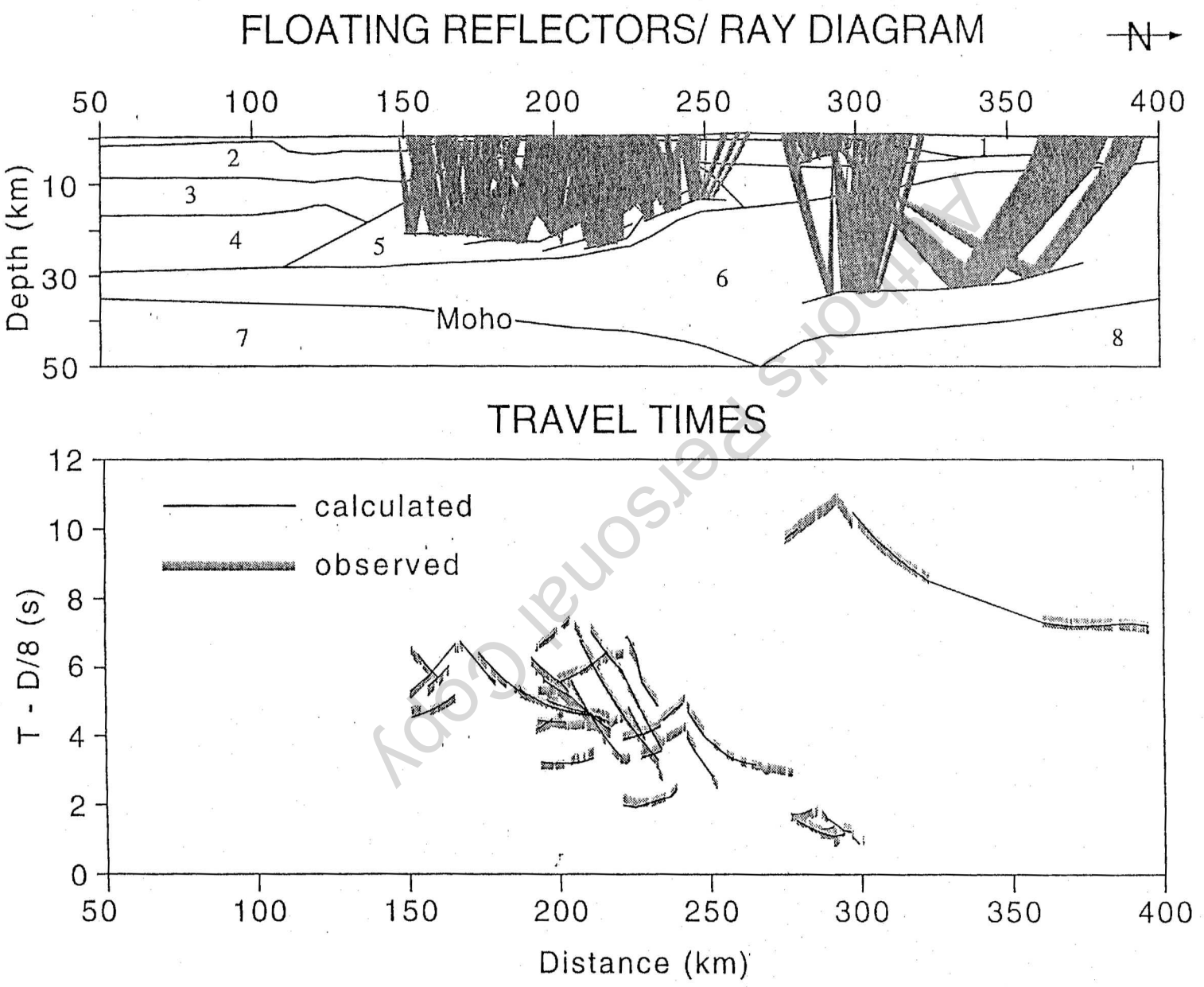
FLOATING REFLECTORS/ RAY DIAGRAM
N
50
100
150
200
250
300
350
400
Depth (km)
10
30
50
2
3
4
5
6
7
8
Moho
TRAVEL TIMES
calculated
observed
T - D/8 (s)
12
10
8
6
4
2
0
Distance (km)

Figure 5g.

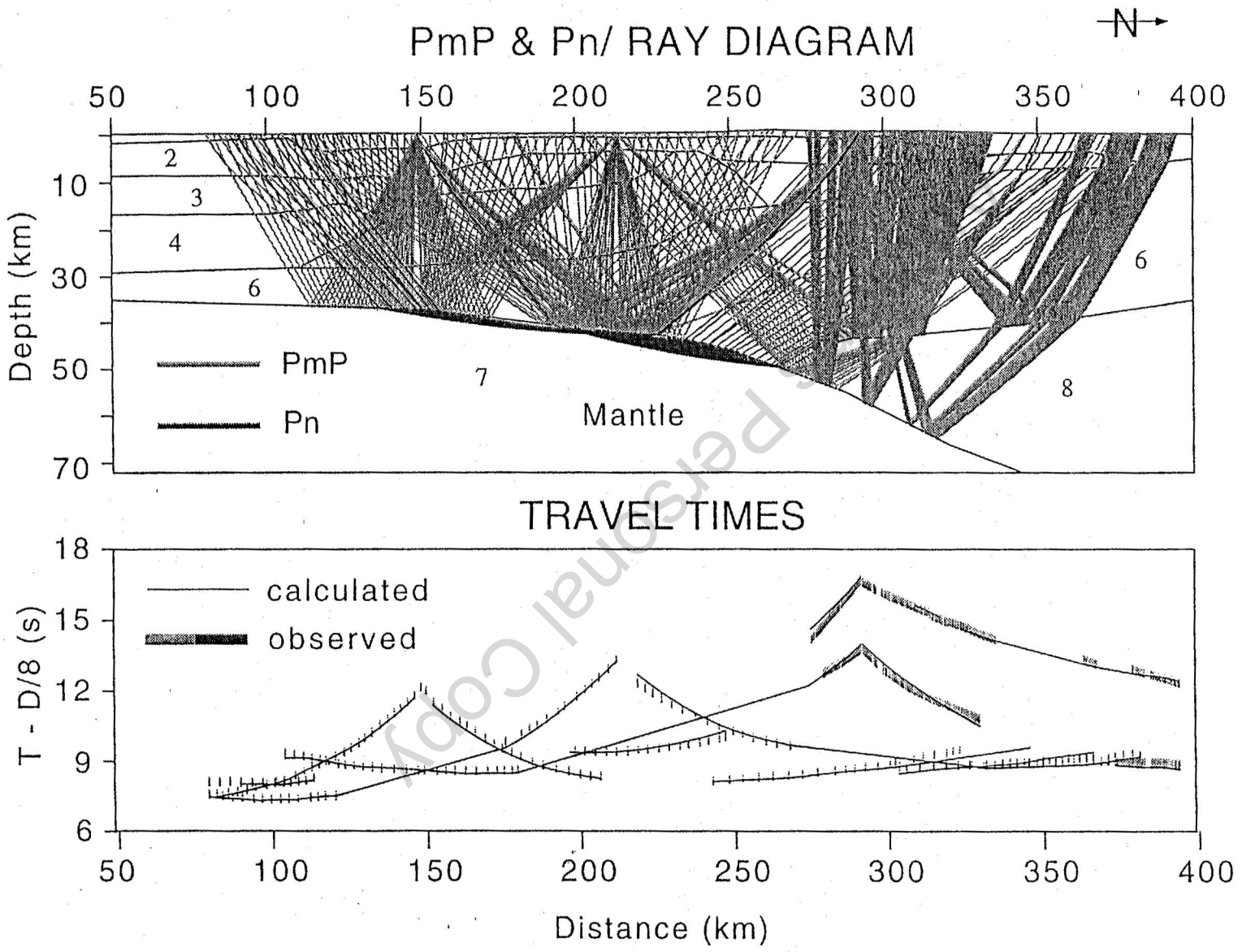
PmP & Pn/ RAY DIAGRAM
N
50
100
150
200
250
300
350
400
Depth (km)
10
30
50
70
2
3
4
6
6
7
8
Mantle
PmP
Pn
TRAVEL TIMES
18
15
12
9
6
T - D/8 (s)
calculated
observed
50
100
150
200
250
300
350
400
Distance (km)

Figure 5h.

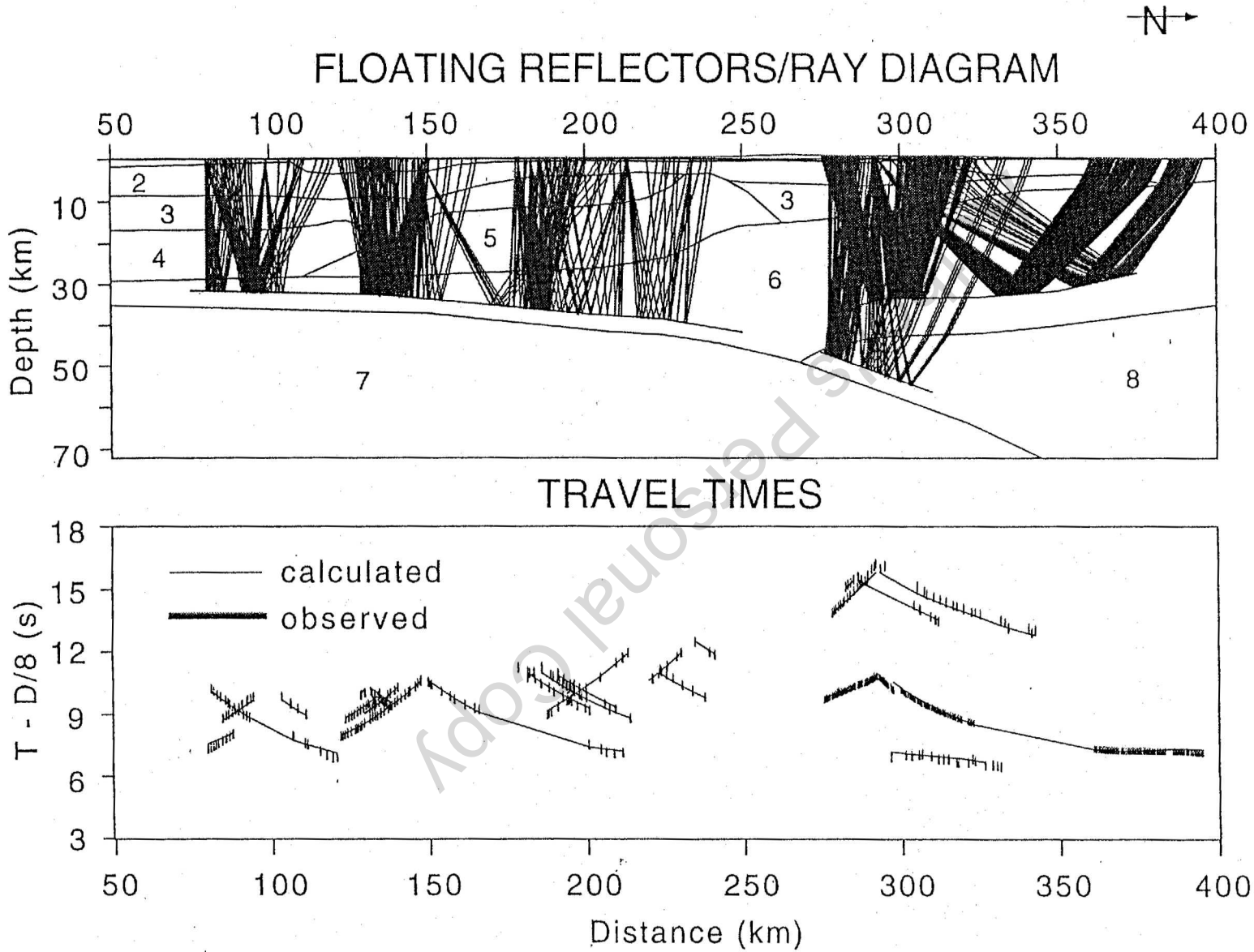
N
FLOATING REFLECTORS/RAY DIAGRAM
50
100
150
200
250
300
350
400
Depth (km)
10
30
50
70
2
3
4
5
3
6
7
8
TRAVEL TIMES
calculated
observed
18
15
12
9
6
3
T - D/8 (s)
50
100
150
200
250
300
350
400
Distance (km)

Figure 5i.

**Figure 6.** Velocity-depth functions with petrophysical data superimposed. (a) The velocity profile at 350 KM in the Colville basin shown with petrophysical measurements from four post-Devonian North Slope sedimentary lithologies (open symbols) and their averages (large solid squares). Velocities from two well logs from North Slope wells are shown dotted. (b) Velocity profile from the EMA at 268 KM with petrophysical data from six EMA lithologies shown as open symbols. The average for EMA samples is shown as large solid squares, that for post-Devonian North Slope sedimentary rock samples is shown as large solid triangles, and that for Doonerak rocks is shown as large solid circles. (c) Velocity profile from the Doonerak area at 245 KM with petrophysical data from two Doonerak lithologies shown as open symbols. The average for Doonerak samples is shown as large solid squares, and that for EMA samples is shown as large solid triangles. (d) Velocity profile from the Skajit at 215 KM with petrophysical data from two Skajit lithologies shown as open symbols. The average for Skajit samples is shown as large solid squares, that for schist belt samples is shown as large solid triangles, and that for Doonerak samples is shown as solid circles. (e) Velocity profile from the schist belt at 180 KM with petrophysical data from two schist belt lithologies shown as open symbols. The average for schist belt samples is shown as large solid squares, and that for Doonerak samples as large solid triangles. (f) Velocity profile from the schist belt at 180 KM with petrophysical data showing the range in velocities of the highly anisotropic schist belt rocks (velocities along orthogonal axes for schist belt rocks are given in Table 2). Average velocities for schist belt rocks are shown as large squares.



Figure 6a.

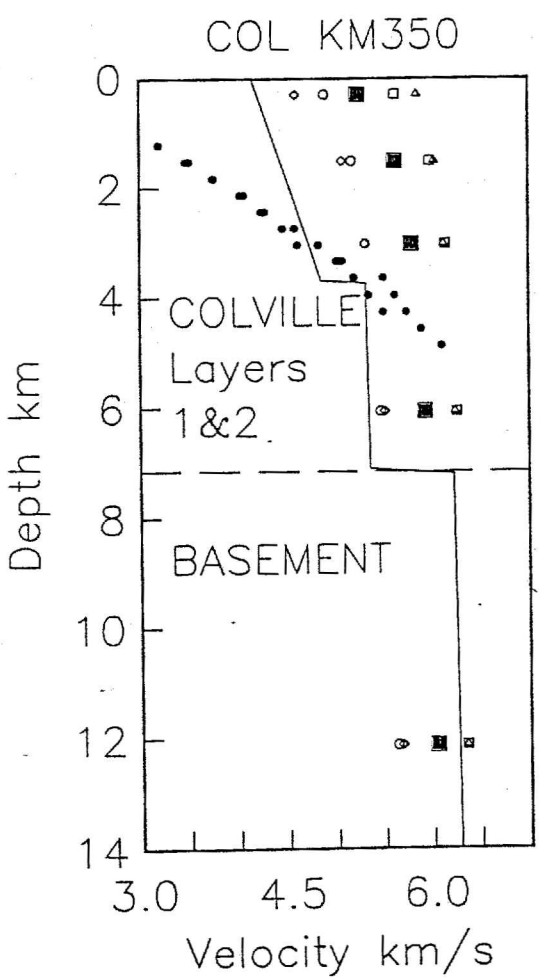


Figure 6b.

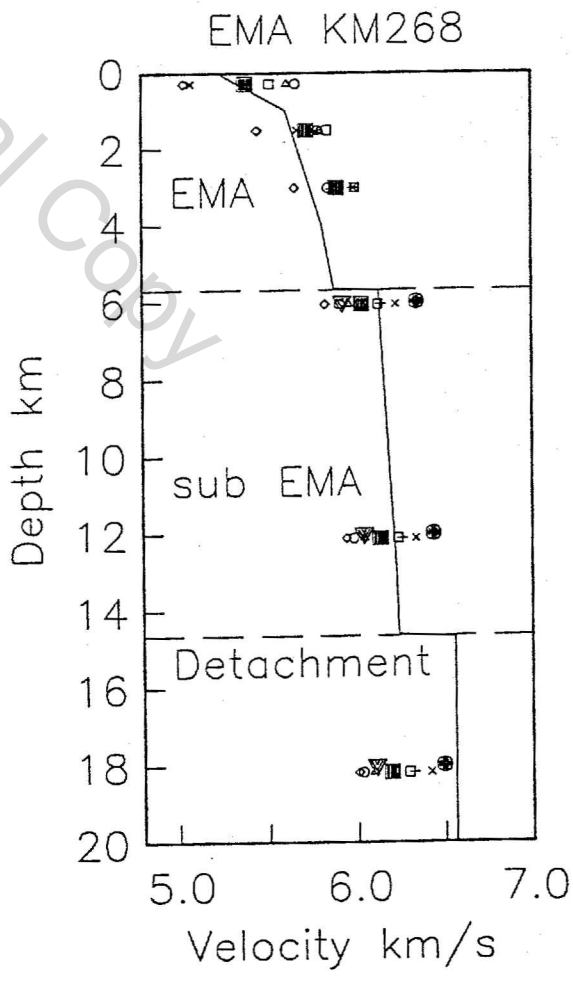

Figure 6c.

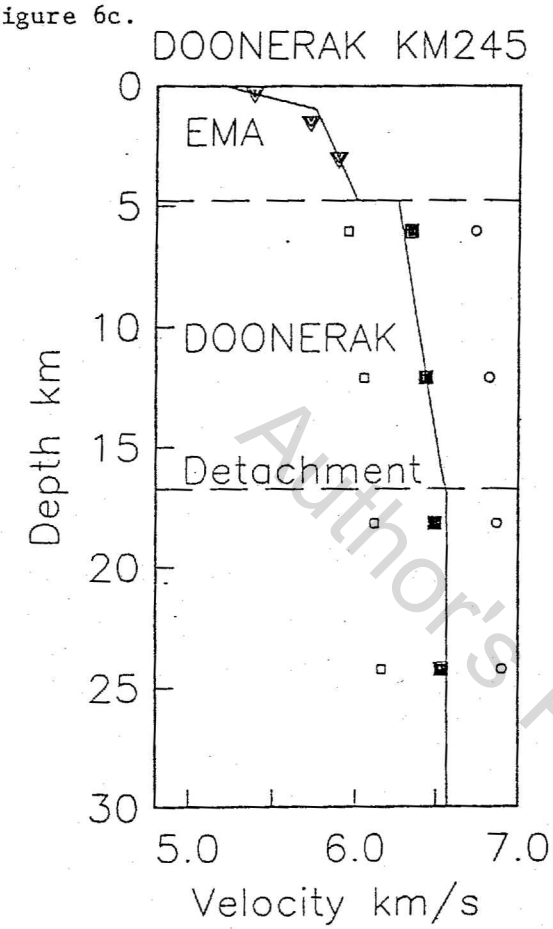


Figure 6d.

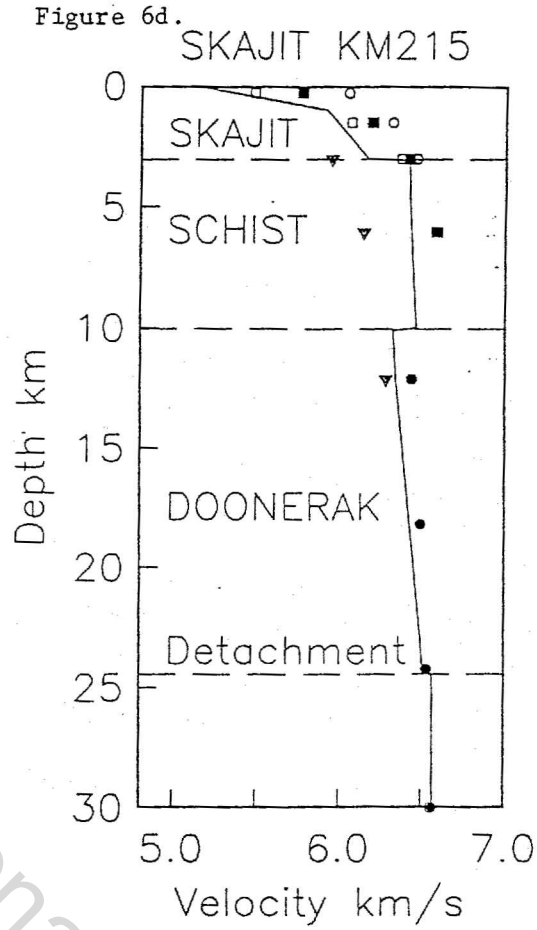


Figure 6e.

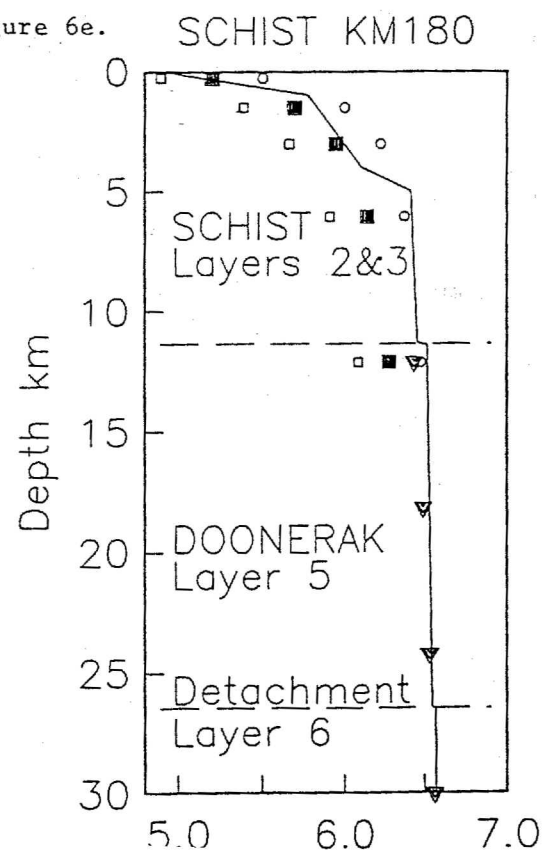


Figure 6f.

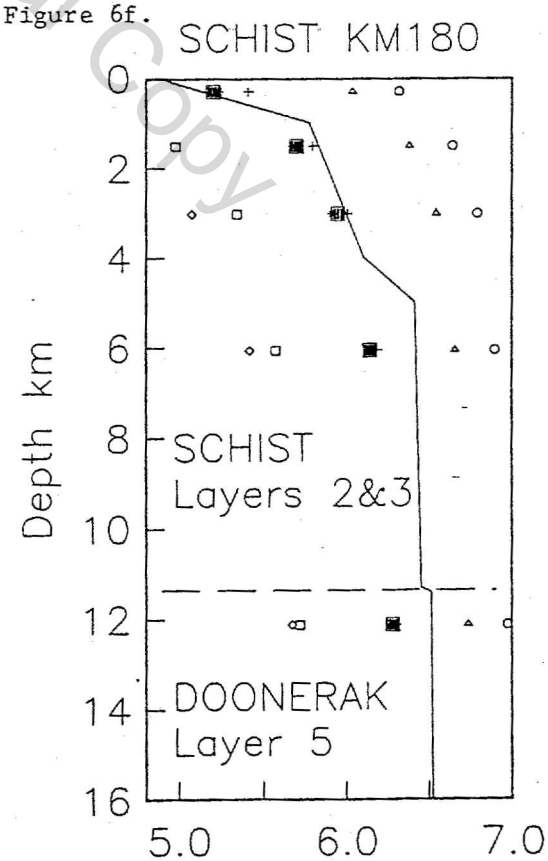

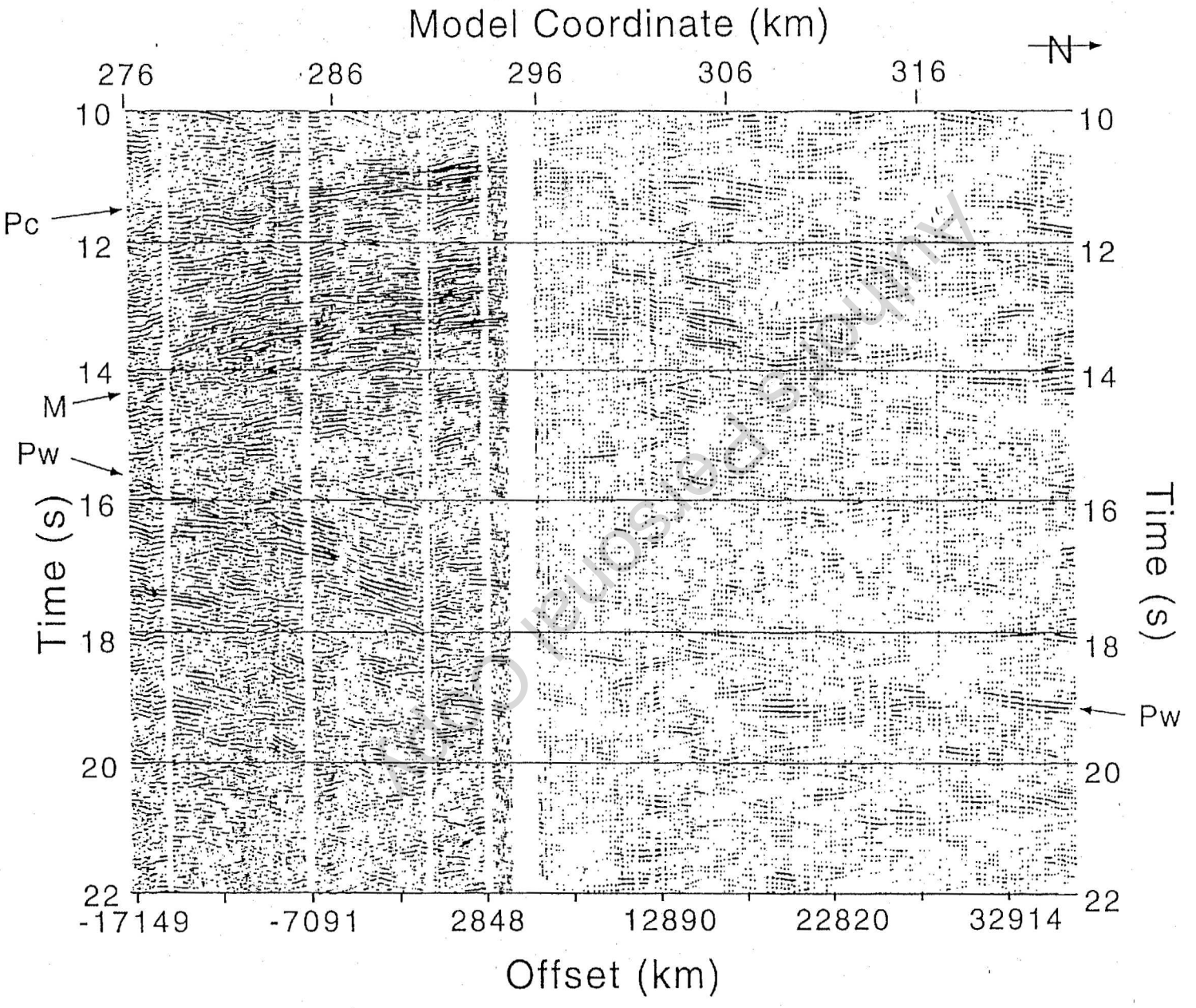


**Figure 7a.** Portion of near offset shot record from shot point 140 (292 KM) showing the double "*PmP*" reflection near beneath the EMA. *Pc* is the top of the reflective lower crust north of the crustal root; the deep reflection is labeled Pw.

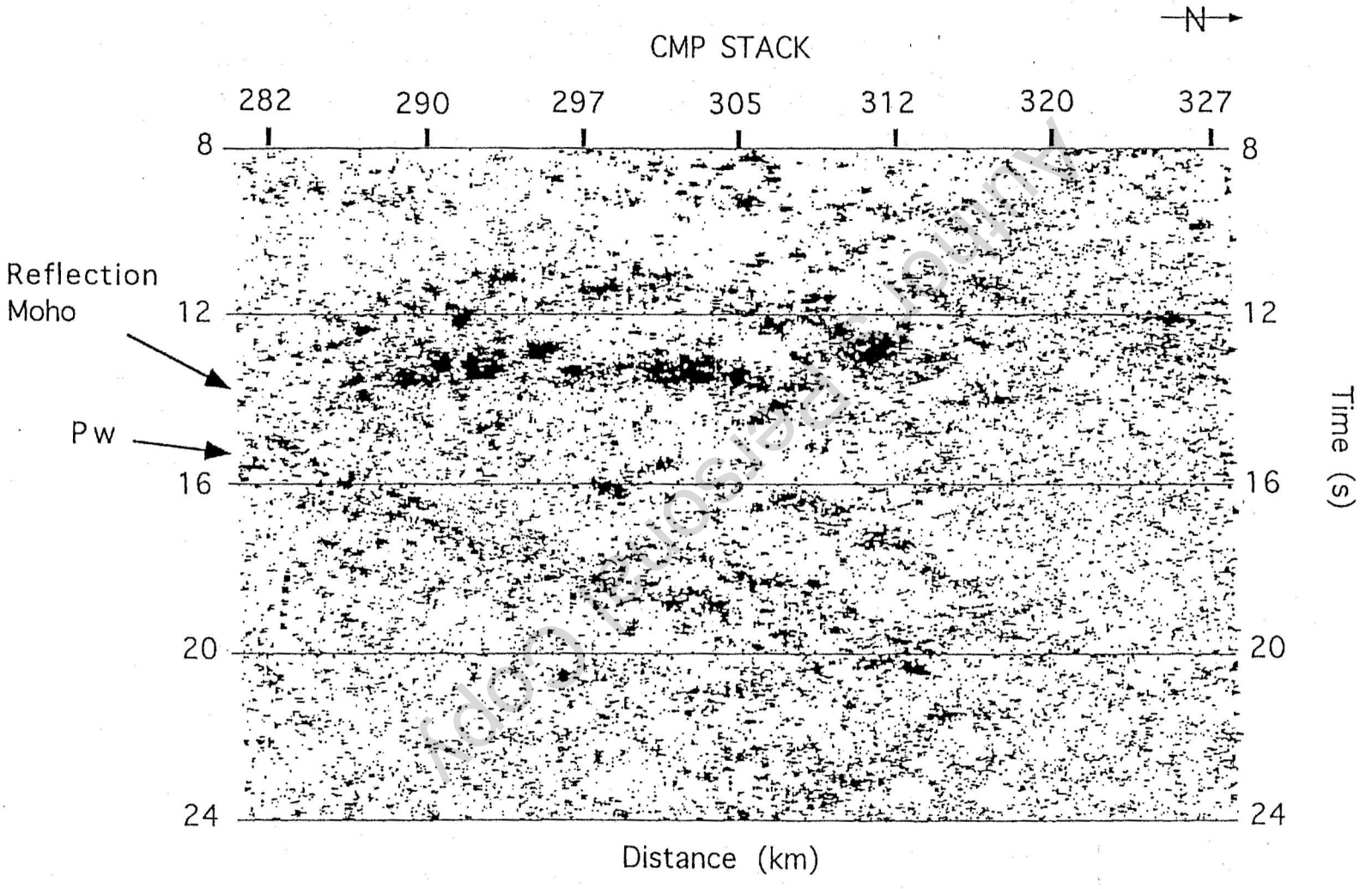


**Figure 7b.** A three shot stack of the Moho beneath the range front and the underlying mantle reflection. The stack was made from offsets less than 35 km. The stack shows an upper layer of reflectivity at 10-14 s, which we interpret as the lower crust and Moho beneath the Colville basin, and a 1.0-1.5 s zone of reflections dipping beneath it from ~16 s at 280 KM to ~20 s at 312 KM. Another band of reflections appears above this at ~16.5 s 305 KM to 21 s 325 KM, suggesting a complicated subduction history.

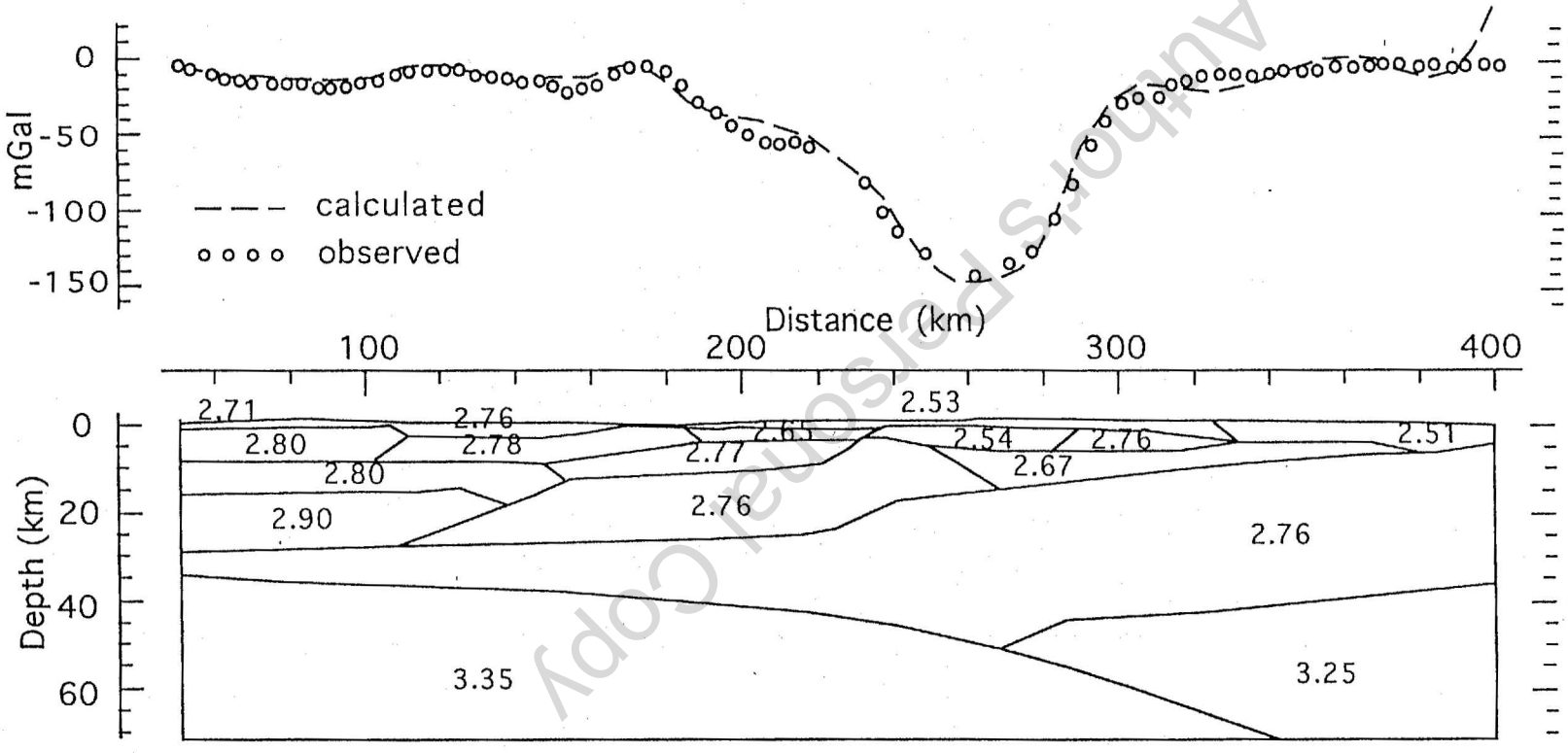




**Figure 8a.** Bouguer gravity data [B. Morin and J. Cady, unpublished data, personal communication, 1995] and gravity model of the Brooks Range derived from the velocity model. Model and final densities (in $10^3$ kg/m$^3$) without crustal densities in the continental subduction zone.

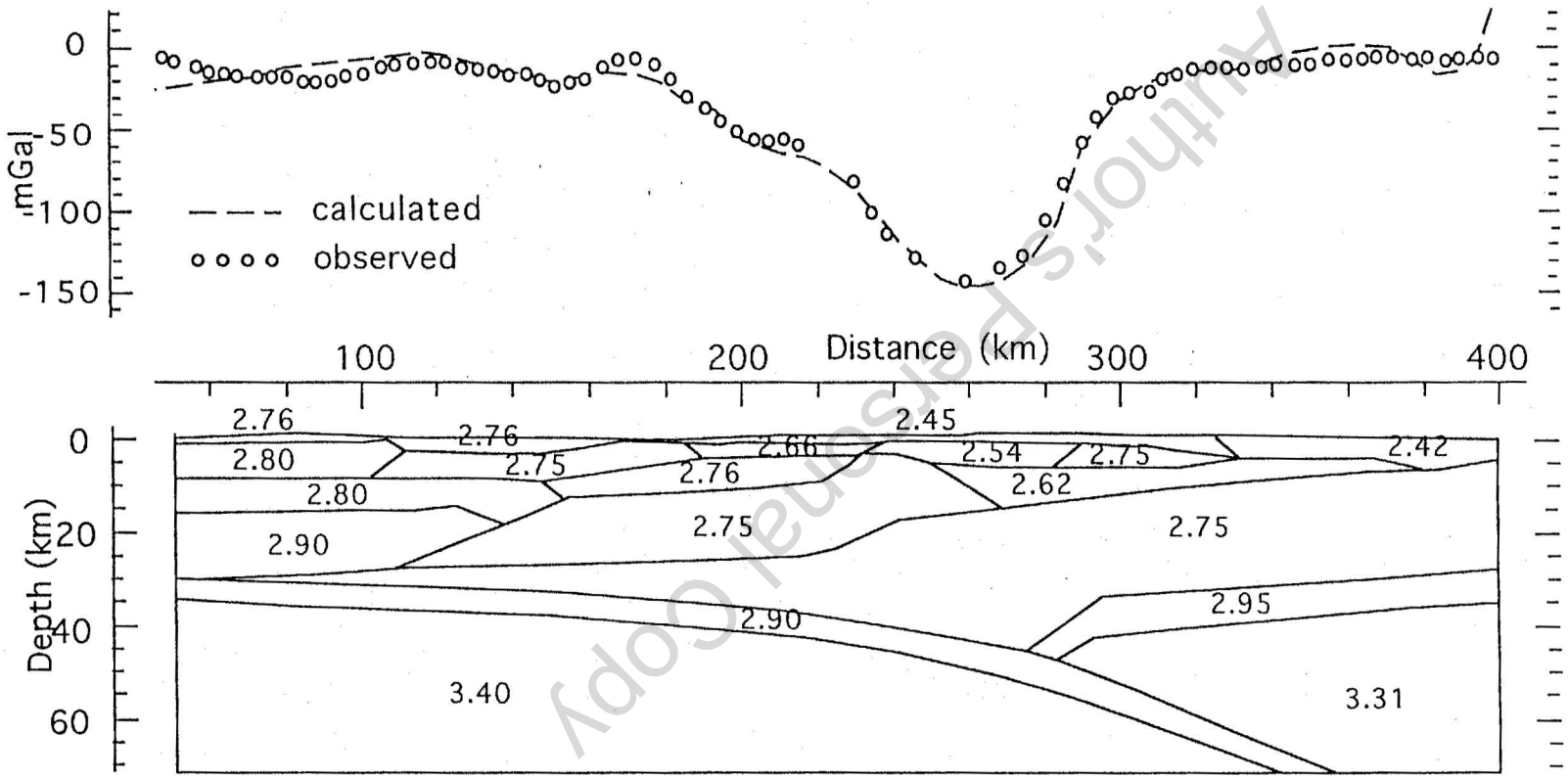




**Figure 8b.** Model and densities with lower-density crustal rocks in the continental subduction zone.

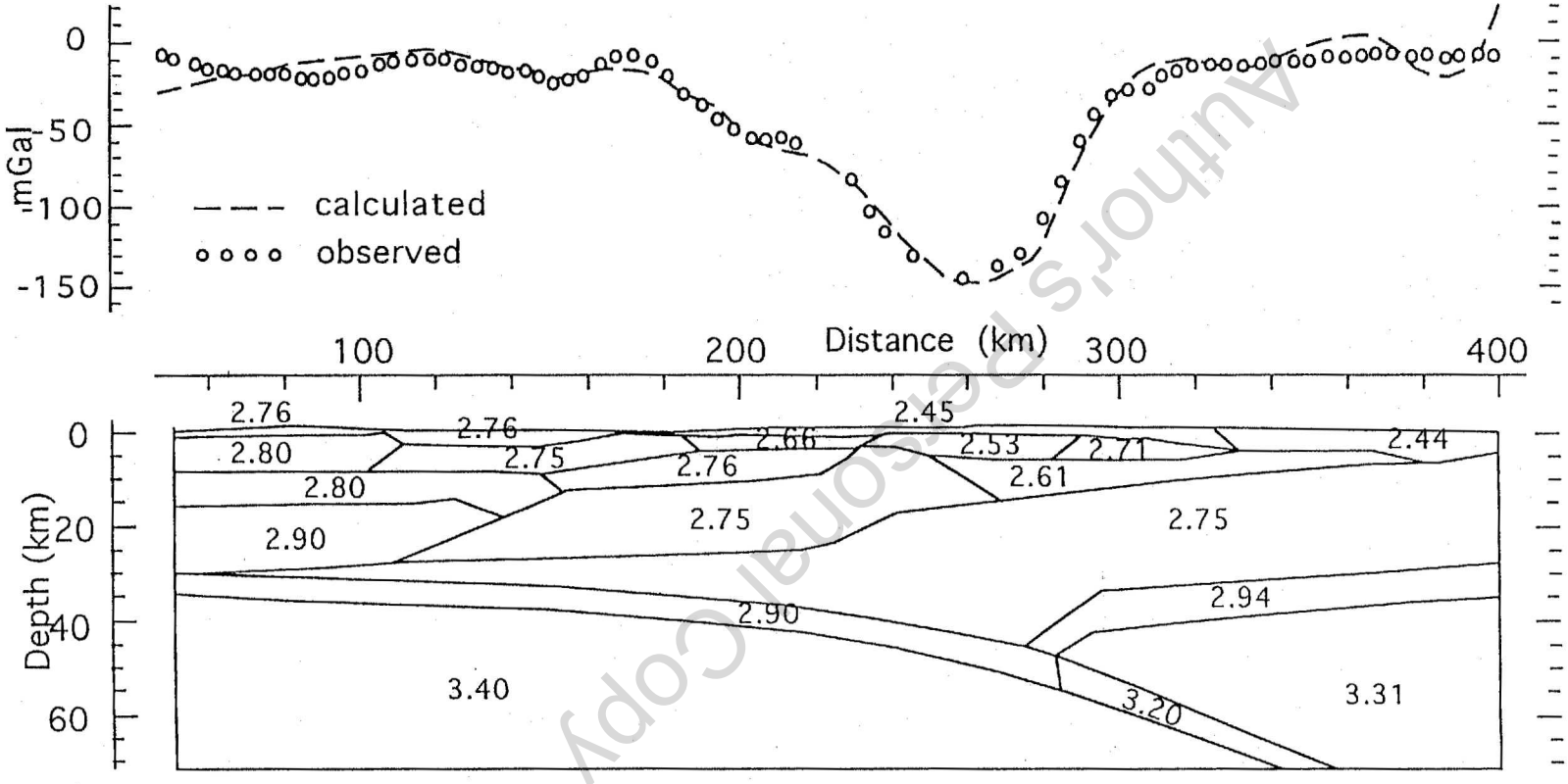




**Figure 8c.** Model and densities with high-density, eclogite facies rocks in the continental subduction zone.

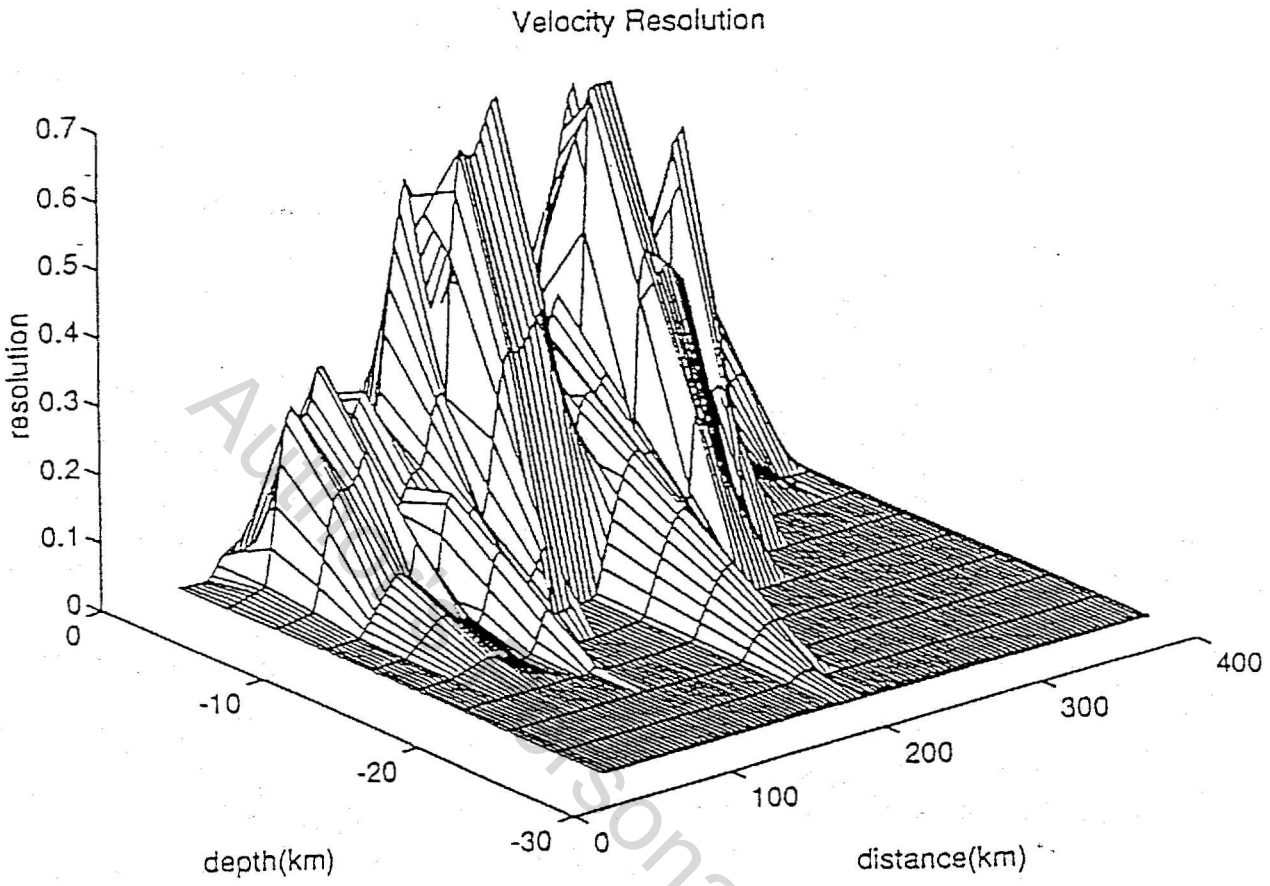




**Figure A1.** Diagonal of the resolution matrix for the velocity parameters determined by inversion of *Pg*. Velocities are best resolved in the center of the model above 10 km depth. Reduced ray coverage across instrument deployment boundaries results in notches in the resolution peaks.